Structure Property Relationship in Rare Earth Based Intermetallics

A Thesis

Submitted in partial fulfilment for the degree of

Master of Science

as part of Integrated Ph.D. programme in Materials Science

By

Mr. Ashutosh Kumar Singh

Chemistry and Physics of Materials Unit

Jawaharlal Nehru Centre for Advanced Scientific Research

(A Deemed University)

Bengaluru – 560064

(INDIA)

March-2019

Dedicated

To my Family and Friends

Declaration

I hereby declare that the matter embodied in the thesis entitled "**Structure Property Relationship in Rare Earth Based Intermetallics**" is the result of investigations carried out by me at the Chemistry and Physics of Materials Unit, *Jawaharlal Nehru Centre for Advanced Scientific Research*, Bengaluru, India under the supervision of **Prof. Sebastian C. Peter** and that it has not been submitted elsewhere for the award of any degree or diploma.

In keeping with the general practice in reporting scientific observations, due acknowledgement has been made whenever the work described is based on the findings of other investigators. Any omission that might have occurred by oversight or error of judgment is regretted.

Ashutosh Kumar Singh

Date:

Bengaluru, India

Certificate

I hereby certify that the matter embodied **in this thesis entitled** "**Structure Property Relationship in Rare Earth Based Intermetallics** " has been carried out by **Mr. Ashutosh Kumar Singh** at the *Chemistry and Physics of Unit, Jawaharlal Nehru Centre for Advanced Scientific Research*, Bengaluru, India under my supervision and that it has not been submitted elsewhere for the award of any degree or diploma.

Prof. Sebastian C. Peter
Associate Professor
New Chemistry Unit
JNCASR
(*Research Supervisor*)

Date:

Bengaluru, India

Acknowledgements

I wish to express my heartfelt gratitude to my research supervisor Prof. Sebastian C. Peter for his guidance, enormous support and encouragement to be free in scientific thoughts. I will always cherish the frankness and enthusiasm with which he has guided me during my MS endeavour. I am greatly indebted to him for mentoring me with infinite patience during this wonderful journey with the SCP lab.

I express my deepest regards and gratitude to Prof. C. N. R. Rao for being the epitome of inspiration and for his unconditional support & affection. It has been a wonderful privilege to be encouraged by a great scientific mind like him at the beginning of my research career. Being in JNCASR provided a great opportunity to observe an iconic figure like him closely, listen to his delightful motivational words and draw constant inspiration from him.

I am thankful to all my course instructors Prof. Umesh Waghmare, Prof. Chandrabhas Narayana, Prof. S. Balasubramanian, Prof. M. Eswaramoorthy, Dr. Sarit S. Agasti, Prof. Kanishka Biswas, Prof. Sebastian C. Peter, Prof. A. Sundaresan, Prof. Alok Chakraborti, Prof. Swapan K. Pati, Prof. Rajesh Ganapathy, Prof. Sobhana Narasimhan, Prof. N. S. Vidyadhiraja and Prof. N. Ravishankar (IISc) whose courses have been extremely helpful.

I would like to sincerely thank all my collaborators: Prof. Dariusz Kaczorowski (Poland), Prof. Marie-Aude Measson (France), Prof. Sudhindra Rayaprol, Dr. Debarchan Das, Dr, Amit Pawbake for measurement research collaborations and their fruitful scientific discussions.

I would specially like to thank Dr. Soumyabrata Roy and Mr. Dundappa Mumbaraddi for fruitful discussions and introducing to crystallography and structure solving.

I would like to thank all the funding agencies like, JNCASR, DST, Synchrotron facilities at PETRA III, DESY (Germany), Elettra (Italy), without whose support, it would have never been possible to conduct research.

I am also greatly thankful to the technical staff members of JNCASR, namely, Mrs. Usha, Mr. Vasu, Mr. Anil, Ms. Selvi, Dr. Joy Ghatak, Mr. Mahesh, Mr. Jagadish, Mr. Shivakumar, for their help with instruments and measurements.

I am thankful for the wonderful support I got from Hostel, Library, Complab, Security, Dhanvantari, Academic Section and Administrative staff for providing and maintaining the great facilities of the centre and make my stay at JNCASR a pleasant one.

I will always remain indebted to the my Lab Family: **Present members**: Dr. Soumyabrata, Dr. Ramarao, Saurav, Shreya, Arjun, Debabrata, Manoj, Risov, Dr. Rajamani, Jithu, Bitan, Devender, **Past members**: Dr. Kanagaraj, Dr. Sumanta, Dr, Subba, Rajkumar, Dundappa, Vamsee, Dr. Vijaykumar. I would particularly like to thank Dr. Ramarao, Saurav, Dundappa, Debabrata for their incessant support and help.

Life at JNC would not have been more memorable without Shashank, Nijita, Pragya, Raagya, Tarandeep, Brijesh. Special thanks to Monis, Momin, Manswee, Reetendra, Mehraj, Narendra, Navneet for making life enjoyable.

I want to convey my gratitude to Dr. Ashly Sebastian for being a wonderful host and for her undying enthusiasm for lab trips and parties. I sincerely thank her for being encouraging, always. I express my heartfelt love and affection to the little angels, Angelyn and Caitlyn.

I am thankful to my volleyball group in JNCASR, for keeping the dream alive of playing volleyball throughout my life and also for being such a nice company

The central spirit of JNCASR and the student community for makinf this journey so memorable.

My brothers and the entire family for their unconditional support.

Thanks to my parents for making me what I am today

Preface

The underlying motivation of thesis is to synthesis new intermetallics and establishes the structure property relationship, which is one of the fundamental questions asked by scientific community. In this process we could able to synthesize two new ternary intermetallic compounds and established their structure property relationships. The structure property relationships were established by means of X-ray diffraction, X-ray Absorption Near Edge Structure analysis, Field Emission - Scanning Electron Microscopy, Mössbauer spectroscopy, Magnetic and Resistivity measurments.

This thesis has 4 chapters. The first chapter discusses about a brief history of intermetallics, its development, synthetic strategy and fundamental properties. Chapters 2 and 3 discuss about the synthesis of new intermetallic compounds. VNiSn is a new intermetallic compound reported in chapter 2, which explains the effect of Ti substitution as well. In chapter 3, a new solid solution Yb_2CoIn_3 synthesised inspired from the earlier work on RE_2TX_3 (*RE* - Rare earth metals, *T* - Transition metals, *X* - main group elements) and their diverse physical properties. This compound exhibited ferromagnetism at room temperature and showing indication of Knodo lattice behavior. Chapter 4 describes the physical properties of an earlier reported compound Eu_2AgGe_3. This compound shows the signature of spin glass behaviour along with low temperature magnetic ordering. Eu_2AgGe_3 exhibits the re-entrant spin glass behaviour, which is, to the best of our knowledge, the first Eu based intermetallics.

Table of Contents

Chapter 1

Introduction

1.1 Background and Motivation

Solid state chemistry is integral part of past and modern-day research. This field came into existence in ~1950s and ever since this field is growing. In earlier days solid state chemistry was dominated by mainly ionic compounds such as transition metal-based oxides, sulphides, nitrides, borides, phosphides and chalcogenides. These material gives the opportunity for physicists and chemist to come across the table as they show very interesting physical properties specially in case of oxides[1–3]. One of the most important phenomenon high temperature superconductivity in cuprates and still research is going on[4]. Later the less ionic intermetallic compounds were also reported for their interesting phenomenon. Specially, rare-earth (*RE*) based intermetallics gives the battleground of theoreticians and experimentalist to understand some basic concept of spin-orbit coupling, highly correlated localized *f*- electrons and their interaction with conduction electrons and competition between all sorts of interaction results in various interesting phenomenon like superconductivity[5–7], heavy fermion[8,9], Kondo behaviour[10,11], spin-liquid behaviour[12,13], etc. These interactions between can be modulated by doping[5], substitution of any foreign element[14] or by some external pressure[14] and magnetic field[15]. Intermetallics are not only fascinated for physical properties but they are also rich in structural chemistry. There are wide variety of crystal system exist like AlB_2[16], $BaAl_4$[17] and their derivative crystal structure which are related through group-subgroup relationships. Ternary derivative of this structure type of comprising *RE*, transition metal (*T*), main block element *X* crystallises in there several superstructures. It depends on the number of atoms in unit call, ratio of number *RE*, *T* and *X* atoms, electron count, chemical nature, solubility limit of elements. Sometimes it leads to the formation of solid solution and disordered phase also. Major problem in this system is unavailability of good quality single crystal to study their anisotropic properties and their phase purity.

The work presented in this thesis was motivated by the above challenges and fascinating properties of these type of systems. In this thesis we focussed on the study of syntheis and structure-property realtionship of *RE* based intermetallic compounds. In three chapters we discuss about the syntheis, structure and properties of VNiSn, Yb_2CoIn_3 and Eu_2AgGe_3 discussed in detail. Amoung them VNiSn and Yb_2CoIn_3 are reporting for the first time. Sample purity and crystal structure was studied by powder and single

crystal XRD measurements. The local structure was studied by Mossbauer spectroscopy and X-ray Absorption Fine Structure (XAFS). Physical properties were studied by magnetic and resistivity measurements.

1.2 Intermetallics

Intermetallic are compound containing at least two different metal and their crystal structure differ from their constituent elements crystal structure. Bonding nature of intermetallics also varies from their constituent's element. In intermetallic, bonding is the mixture of covalent and ionic nature resulting in directionality in bonding. On the other hand in metals due to their delocalized (free) electrons form metallic bonding that leads to non-directionality in bonding. Change in crystal structure and bonding nature gives fascinating physical and chemical properties. Intermetallics have found application in various fields ranging from high temperature superconductivity, strange magnetic behaviour, host for kondo-behaviour, heavy fermions, charge density waves, spin-glass behaviour to the catalyst in Hydrogen evolution reaction (HER), oxygen evolution reaction (OER), sensor and thermoelectric materials as it was mentioned above. However, intermetallic compounds are given the second eye as compared to relatively more ionic systems like oxides, ceramics, halides and metal chalcogenides. This secondary attention attributed to the difficulty in understanding the basic understanding of composition, bonding nature, assignment of the oxidation state of compositional atoms and an interpretation of the origin of any physical phenomenon.

Intermetallic compounds are rich crystal chemistry. Intermetallics compounds crystallises in more than 2166 structure types out of which 943 binary while most in ternary and very few in other phases. More than 1495 ABC (chemical composition) ternary intermetallic compound is reported. Based upon the atomic element, atomic size and oxidation number their crystal structure is varying.

1.2.1 Classification

1.2.1.1 Polar intermetallics and Zintl Phase

Polar IMs are compounds comprises early transition metals with p-block elements. Transition metals behave as cation and p-block elements as a counterpart anion due to great amount of electronegativity difference. These structures are highly condensed and connected to each other owing to smaller ratio of p-block elements[20]. A slightly related class is Zintl phase, which have some basic criteria to be classified as

1. Zintl phase should contain at least alkali metals or alkaline earth metals/*RE* metals and p-block elements

2. These materials are should be electronically neutral
3. Generally, all Zintl phase compounds are narrow band gap semiconductor.

There are several compounds in are known to exist in Zintl phase family[21]. They have found particularly interesting for thermoelectric materials[22].

1.2.1.2 Heusler Phase

Heusler phase was first synthesized 1903 in the form of Cu_2MnAl by Fritz Heusler. Heusler system can be generalized as X_2YZ where X and Y atoms are cationic in nature and Z as anionic counterpart. Heusler system crystallize in $Fm\bar{3}m$ cubic space group. This structure can be imagined as four interpenetrating sublattice consisting of face cantered cubic NaCl and zinc blende structure of ZnS. Half-Heusler system having general formula XYZ crystallise in $F\bar{4}3m$ and can be derived from the Heusler system by removing the one atom X. A detailed review on Heusler system and their physical properties is written by Graf et. al[23]. Relation between Heusler and Half-Heusler is plotted in **Figure 1.1**

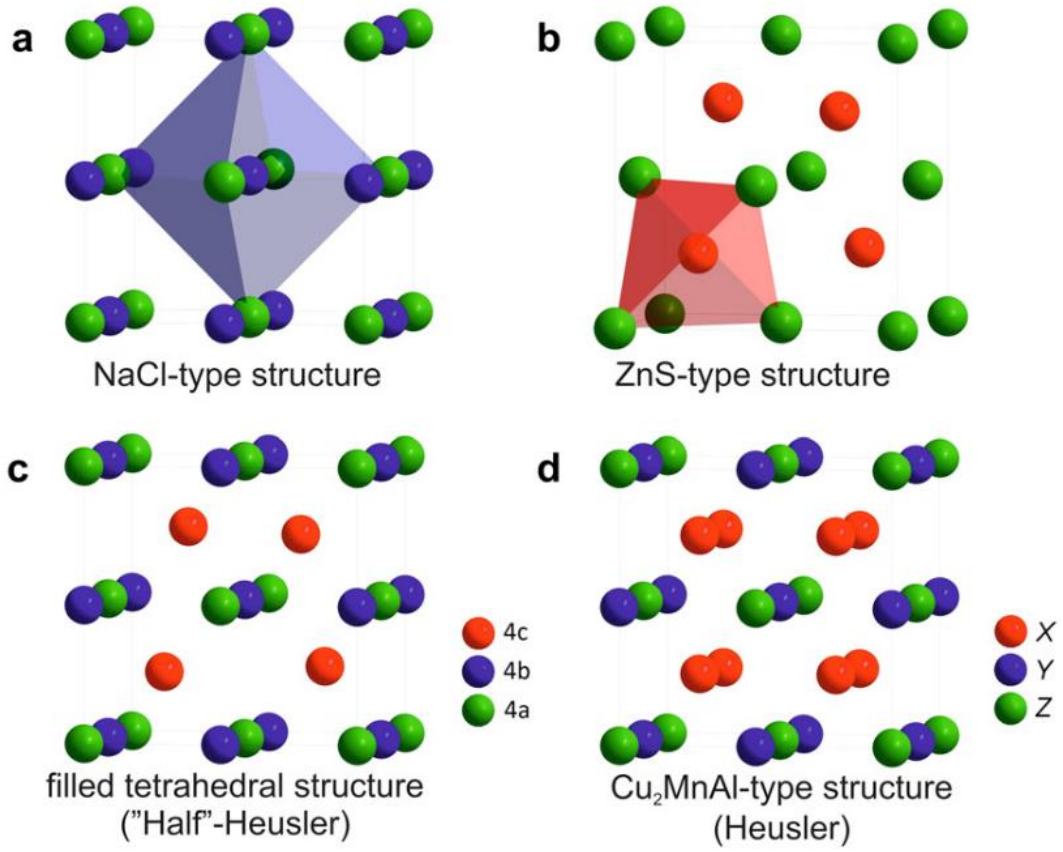

Figure 1.1. (a) Rock salt structure, (b) zinc blende structure and their relations to the Half-Heusler structure (c), and to the Heusler structure (d). **(Reproduce with permission from Progress in Solid State Chemistry)**

1.2.1.3 Samson Phase

It is very unusual class of IM which contain very high number of atoms in unit cell. β-Mg_3Al_2 was first IM to be reported as Samson phase[24] and crystallise in cubic $Fd3m(O^7_h)$. It consists of 1168 atoms which distributed among the 1832 atomic position. β-Mg_3Al_2 constructed from the fused truncated polyhedra of different size.

1.2.1.4 Hume-Rothery Phases

Cu-Zn a alloy first recognised by Hume-Rothery, describe it as binary metal alloy on their mean valency. However, later there are some rules should be followed to classify a compound as Hume-Rothery phase just like in case of Zintl phase. Here are the following criteria for Hume-Rothery phase[25];

1. Difference between solvent and solute atoms radius is less than 15%
2. Both components exist in same structure type, lesser the electronegativity difference
3. Same structure type, lesser the electronegativity difference
4. Solubility of metal with higher valance should be more than metal of low valency the vice-versa.

1.2.3 Difference between Intermetallic, Bimetallic, Alloys and Solid Solution

IMCs differ from all other in terms of structurally and electronically. IM have the mixture of covalent and ionic nature. While in all bimetallic, alloys and solid solution have non-directionality in bonds due to delocalised electrons. In alloys and solid solution there is no fixed position of solute atom and they randomly occupy in the lattice and they have wide range of concentration. Bimetallic comprises of two metals which form the interface and do not mix with each other. Essentially it forms the heterogeneous mixture[26]. **Figure 1.2** depicts the structural differences between these phases.

1.3 Synthesis of Intermetallics

It is always a great interest to develop the new synthesis method for discovering new materials with some novel properties. In this hunt several different approaches have been developed in the past. However, it is one of the biggest challenges in solid state chemistry of synthesizing a new compound. This difficulty increases manifold in case of IMs due to lack of clear idea of oxidation state and exact composition of IMs as compared to well known ionic family of solid-state chemistry namely oxides, phosphides, chalcogenides and halides. A traditional way of synthesising IMs is to heat the mixture of element in proper stoichiometric ratio at higher temperature. But there has been some

ambiguity in this approach. Sometimes different route for synthesizing a IM lead to different composition and consequently crystallize in different crystal structure. So, a different physical property is expected since all physical properties depends on crystal structure. Therefore, it is more important to grow a single crystal single crystal of desired composition to get the intrinsic property of materials which should be independent of route of synthesis. Now, describing some synthesis method for IMs.

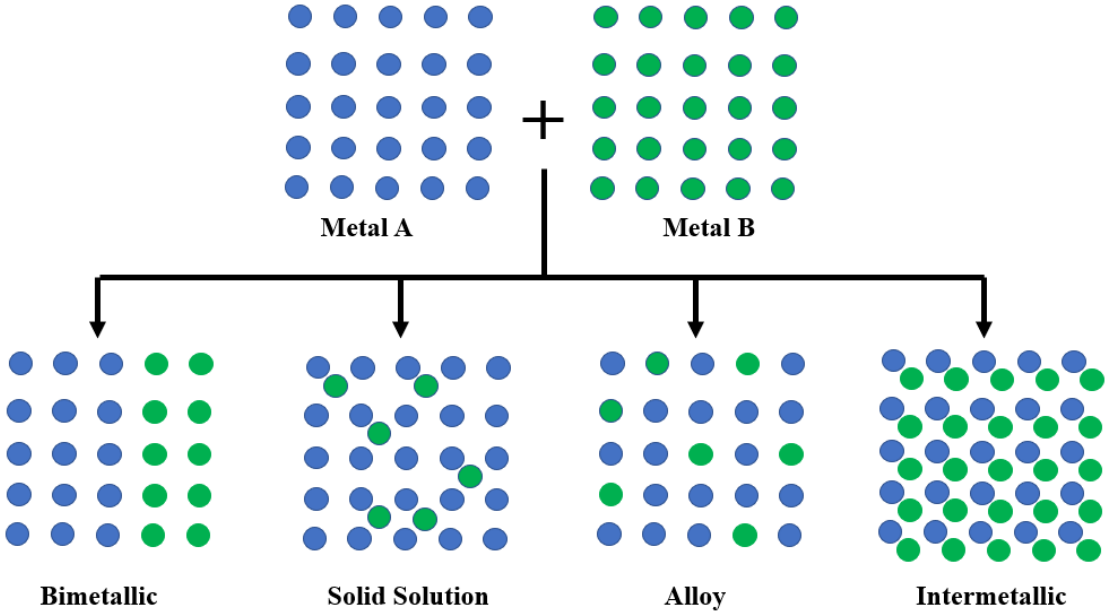

Figure 1.2. Schematic representation of the formation of bimetallic, solid solution, alloy and intermetallic compounds at atomic level.

1.3.1 Ceramic method

It is a traditional method for synthesising bulk intermetallics. It is an example of metallurgical technique which follows as direct heating of constituent elements in evacuated quartz tube at high temperature for long time and followed by prolonged annealing at lower temperature for several days to increase the crystallinity of the sample. This method has been successful for many IMs, but it has some limitation. Sometimes it is difficult to get the desired homogeneous composition of materials and this method is time consuming.

1.3.2 Arc Melting

This is also a traditional method for the synthesis for IMs and has some great advantage over ceramic method. Arc-melting is one of the quickest methods to synthesize IMs. One more great advantage it has over other technique it can reaches the temperature till 3000 K in seconds which give it upper hand for synthesising some metals with very

high melting point like W, Pt and Pd metals. A typical Arc Melter MAM-1 developed by Edmund Bühler GmbH is shown in **Figure 1.3**

Figure 1.3 MAM-1 Arc Melter designed by Edmund Bühler GmbH.

But this method also has disadvantage over other methods in synthesis of low vapour pressure like Eu and Yb. Since Arc-Melting method is quasi-open system evaporation can badly affect the synthesis of pure compound. To get a perspective, synthesis of YbPtSn by arc melting technique since Pt (m. p. 2045 K) is much higher than Yb (b. p. 1469 K) so before reacting to each other all the Yb metal will evaporates and synthesis of YbPtSn is not possible.

1.3.3 High Frequency Induction Heating

Difficulty arises in Arc-Melting can be resolved by High frequency induction furnace heating (FIH). This method utilises one of the principles of ceramic method were all the elements placed in evacuated quartz tube. In this method reactant elements were sealed inside a container of low reactivity and very high melting point like of some alloys of niobium, tantalum or molybdenum. This technique can be improved by coupling with arc melting technique where first the sample can be melted by arc melting and then followed by high frequency induction heating. This system has always been coupled with glass crucible in a water-cooled sample chamber. In this method one can directly observe the reaction through direct transparent observation window. This method mainly used for 4*d*, 5*d* elements and for *RE* based compounds. This solid-state synthesis sometime gives the inhomogeneous mixture and sometime container may react with reactant and gives some impure phase of the compound. A typical HFIH apparatus is shown in **Figure 1.4.**

Figure 1.4. High frequency Induction Heating coupled designed by Ambrell company, U.S.A. coupled with water cooled sample chamber.

1.3.4 Metal Flux method

Although conventional technique such as HFIH can be used for the synthesis majority of the compounds within short period of time, they are limited only for the synthesis of thermodynamically stable products, so it is difficult to access the metastable phases or the structures that are stable at low temperatures. These traditional methods are limited in the synthesis and crystal growth of irregular-shaped single crystals. High temperature methods favour grain growth and the formation of large crystallites of micrometre scale due to the difficulty in controlling the crystallite size and morphology. High quality single growth is important to study the structure-property relationship. It is a well-established fact that physical property measurement on pellets leads to homogeneity in the property (no anisotropy measurement) as well as no intrinsic property. Metal flux method has not only been proved to be a tremendous tool to grow single crystals of already known polycrystalline compounds for studying detailed physical properties but also been an effective way to explore completely new compounds[27–29]. One of the interesting features of the metal flux synthesis method is in the reduction of melting point and vapor pressure of the starting materials, which resulted in the formation of new compounds. A review about the concept and use of metal flux technique for the formation of new compounds was reported by Kanatzidis and co-workers and has been demonstrated that molten metal fluxes represent an excellent alternative to the conventional synthetic methods for the exploratory synthesis of new *RE* based IMs[25].

1.4. Physical Properties of Intermetallic

A broader picture of physical properties of intermetallics has been given in motivation part of the introduction and how much they are rich in physics and chemistry.

In the following part there will be broader view of some of the physical properties will be discussed.

1.4.1 Magnetism

Magnetism has a very rich history in terms of its development. Magnetic materials can be classified as diamagnetic, paramagnetic, ferromagnetic, antiferromagnetic, ferrimagnets. The fundamental description of each one can be seen in Kittel's book[30]. Diamagnetic materials exhibit temperature independent negative magnetic susceptibility (χ), while positive susceptibility is evident in paramagnetic system, which follows the inverse relation with temperature (Curie's law). In diamagnetic materials, magnetic moment vectors cancel each other while in paramagnetic materials spin are randomly oriented. In case of ferromagnetic materials magnetic susceptibility χ is positive and observed below the characteristic Curie temperature (T_c) and in antiferromagnetic materials magnetic susceptibility χ is positive, observed below characteristic Neels temperature (T_N). In ferromagnetic materials magnetic moments align parallel while in case of antiferromagnetic materials they align in opposite direction. In case of ferrimagnetic materials spins align in opposite direction only but they are out of proportion. A schematic has been shown in **Figure 1.5**

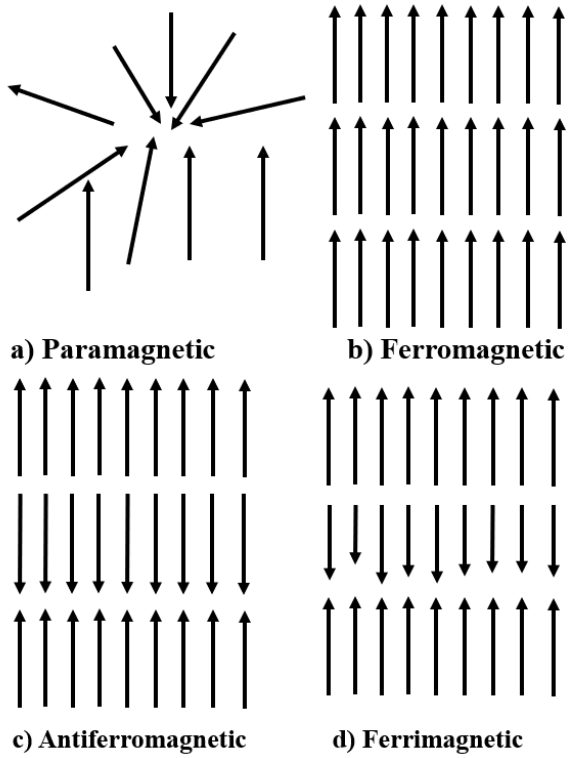

Figure 1.5 schematic diagrams of different kinds of magnetic materials a) paramagnetism, b) ferromagnetism, c) Antiferromagnetism and d) ferrimagnetism.

1.4.2 Spin Glass

Spin glass system can be understood as disordered magnate with geometric frustration. An example of geometric frustration depicted in **Figure 1.5**, which represents a triangular lattice comprises of a magnetic moment at a site aligned in upward direction and another magnetic moment at b site align in downward direction. If the lattice has to behave as antiferromagnetic material, then it spin at site c should align upward according to site b but according to site a it should align in downwards direction. So, in this situation magnetic moment can at site c cannot determine in which orientation it should occupy and system is known as magnetically frustrated.

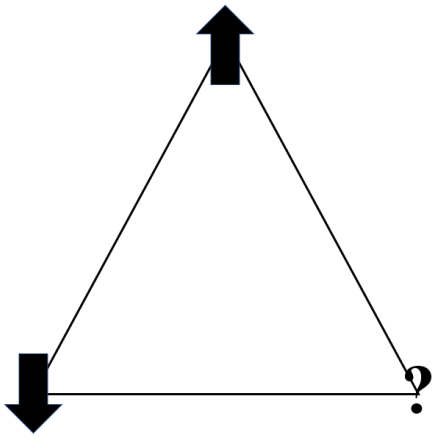

Figure 1.5. Magnetic frustration in triangular lattice and magnetic frustration at lattice site c

1.4.2.1 Theoretical model for Spin Glass

In the following section will be briefly discussing theoretical background of spin glass. Spin glass behaviour is much more complicated than the normal ferromagnetic, antiferromagnetic or any other type of magnetic ordering. So, it necessary to understand the theoretical background in detail.

1.4.2.1 Edwards and Anderson Model

In 1975, Edwards and Anderson (EA) give this theoretical model in which spin S_i are locked into their preferred direction on the crystal lattice with no correlation with over other crystal sites on reducing the temperature[31]. It is example of transition from paramagnetic phase to a frozen ground state like classical theory of Ehrenfest classification for phase transition. Since in frozen state there is no long-range ordering so order parameter of no use. So, Edwards and Anderson came out with a new order parameter called time order. Spin orientation will be same over long period of time. The spin is taken as Ising type. Exchange coupling between them is only nearest neighbour

and these coupling are randomly chosen as Gaussian distribution. This theory predicts there will be cusp in specific heat at the transition temperature but in experiments it was found out be a broader maximum. It also predicts there will be zero residual entropy in the system. This cannot be true since if there is zero residual entropy then there is no possibility of transition, it happens only when there is multiple nearly degenerate ground state. Nevertheless, this theory first gives the theoretical reasoning behind spin glass in simple manner. To overcome this failure Sherrington and Krikpatrick Model came.

1.4.2.2 Sherrington and Krikpatrick Model

Sherrington and Krikpatrick (SK) model is extension of EA model[32]. In SK model they used an approximation using mean field theory (MFT), all the infinite spin in the lattice will interact with each other spins no matter how much they are separated in space. SK model was exactly solvable on this assumption. However, this model also has certain limitation over residual entropy. This theory incorrectly predicts the negative residual entropy. Negative value of residual entropy has no physical significance however it was improved by Parisi, using replica breaking symmetry[33].

1.4.2.3 Experimental evidence of spin glass behaviour

There are multiple ways in which one can verify the spin glass behaviour in the materials. The first indication of spin glass behaviour in materials comes from the bifurcation in ZFC and FC curve in magnetic susceptibility measurement. However, it is not necessary that a system showing bifurcation will be spin glass. An example of this phenomenon is U_2RhSi_3 reported for bifurcation in ZFC and FC curve but there was no sign of spin glass behaviour from other measurement and bifurcation was attributed to ferromagnetic domain wall pinning effect[34]. This type behaviour is also observed in case of superparamagnets. Therefore, ac susceptibility with varying frequency and their effect on variation of peak position is strong tool to classify a material for spin glass behaviour. Isothermal relaxation magnetization is one more tool to get the time parameter which is characteristic of EA model for spin glass. To get the nature of spin glass and their dynamics behaviour μSR spin rotation is an excellent tool[35].

1.4.3. Kondo effect

In a metallic sample there is a linear decease in resistivity on lowering the temperature due to decrease in scattering of conducting electron and this is result of decrease in lattice vibration on lowering the temperature. There is residual resistivity in

the sample due to defects, impurity and vacancy which is independent of temperature since there is no lattice vibration is almost zero. However, in some lattice there is sudden upturn in resistivity in lower temperature range and was first explain by Joule Kondo in 1964[36]. It can be explained by interaction of magnetic impurity element incorporated in metallic lattice. At low temperature, scattering of conduction electron by the magnetic ion which interacts with spins of conduction electrons. It was proposed that in low temperature range the contribution of higher order term is much larger than the first term in resistivity temperature relation.

$$\rho(T) = \rho_0 + aT^2 + \boldsymbol{c_m \ln(\mu/T)} + bT^5$$

Where ρ resistivity, ρ_0 is residual resistivity, second term in accounts for fermi liquid behaviour and last accounts for lattice vibrations. It is the third logarithmic term which comes for what known as Kondo scattering. There are several materials in which Kondo effect has been observed especially of Ce and Yb based system[10,11,36].

1.4.4 Heavy Fermions

Fermions are the particle which follows the laws of Fermi-Dirac statistics. Particle follows the Pauli Exclusion Principle. Electrons are classical example of fermions. When the mass of particle is unusually higher than the normal mass it named as heavy fermions. Heavy fermionic property is exhibited mainly by materials based *f*-block elements having unpaired *f*-electrons and their interaction with conduction electron. Heavy fermions can have different kind of ground state like ferromagnetic, antiferromagnetic, superconducting, conducting or even insulating. This property is characterized specific heat at low temperature. Specific heat of materials can be expressed as

$$C = \gamma T + \beta T^2 + \text{higher term}$$

Where C is total specific heat, γ is electronic coefficient foe electronic contribution specific heat, β is lattice contribution to specific heat. It is the γ (in $mJ/mol.K^{-2}$) value of 0-50, 50-100, 100-1000 and > 10000 to be classified as normal metal, moderate, heavy or classical fermion, respectively.

Heavy fermionic properties in materials come from the interaction of localized *f*-electrons on lattice to conduction electrons to through Kondo exchange interaction which generally yield non-magnetic ground state. It also interacts via Ruderman-Kittel-Kasuya-Yosida (RKKY) oscillatory exchange interaction which generally yields the antiferromagnetic ground state. Some of the Ce based materials classical example of heavy fermions[9,30,37–42].

1.5 Summary

In this chapter we briefly discussed about solid state chemistry and evolution of intermetallics, challenges in synthetic strategy and development of new strategy, their advantage and disadvantage over each other. Classification of intermetallics based on the polarity and structural diversity. Introductory concept of magnetism and their physical picture. A brief introduction of spin glass theory and ways of experimental verification based on the basics of magnetism. Introduction of low temperature physical properties of on intermetallics in the terms of heavy fermions and Kondo behaviour.

The introduction of chapter talks about a brief history of intermetallics, it's development, synthetic strategy and fundamental properties. The underlying motivation of thesis to synthesis of the new intermetallics and establishes the structure property relationship which is one of the fundamental question asked by scientific community. In this process we are able to synthesize two new ternary intermetallics compounds and established their structure property relationship. The structure property relation were established by means of XRD, FE-SEM, Mössbauer, magnetic, resistivity and XANES analysis

This thesis can be divided into two parts. First part comprising of chapter 2 and 3 where synthesis of new intermetallic compound and one solid solution is reported.. In chapter 2, VNiSn new intermetallic compound was studied in great details and effect of Ti substitution on the structure. In chapter 3 a new solid solution Yb_2CoIn_3 synthesised inspired from the earlier work RE_2TX_3 (*RE*- Rare earth metals, *T*- Transition metals, *X*- main group elements) and their diverse physical properties. This compounds is reporting for room temperature ferromagnetism and showing indication of formation of Knodo lattice. Second part of thesis consist of chapter 4. There a earlier reported compound Eu_2AgGe_3, physical properties were studied in detail and preliminary studies show the signature of spin glass behaviour along with low temperature magnetic ordering. Eu_2AgGe_3 exhibits the re-entrant spin glass behaviour, which is for the first time in case of Eu based intermetallics.

References

(1) Cava, R. J. Oxide Superconductors Robert. *J. Am. Ceram. Soc.* **2000**, *83*, 5–28.

(2) Nicol J., Shapiro S., S. P. H. Direct Measurement of the Superconducitng Energy Gap. *Phys. Rev. Lett.* **1960**, *5*, 461–463.

(3) Rao, C. N. R. High-Temperature Ceramic Oxide Superconductors . **1988**, *13* (485), 19–35.

(4) Taillefer, L. Scattering and Pairing in Cuprate Superconductors. *Annu. Rev. Condens. Matter Phys* **2010**, *1*, 51–70.

(5) Davidov, D.; Chelkowski, A.; Rettori, C.; Orbach, R.; Maple, M. B. Electron Spin Resonance and Superconductivity in $Gd_xLa_{1-x}Al_2$ Interemetallic Compounds. *Phys. Rev. B* **1973**, *7*, 1029–1038.

(6) H. R. Ott, F. Hulliger, Fisk, Z.; Rudigier, H. Superconductivity in Uranium Compounds with Cu_3Au Structure. *Phys. Rev. B* **1985**, *31*, 1329–1333.

(7) T. T. M. Palstra, G. Lu, A. A. Mcnovsky, G. J. Nieuwenhuys, P. H. Kes, and J. A. M. Superconductivity in the Ternary Rare-Earth {Y,La, and Lu) Compounds RPd_2Si_2 and $RERh_2Si_2$. *Phys. Rev. B* **1986**, *34*, 4566–4570.

(8) Mito, T.; Kawasaki, S.; Kawasaki, Y.; Kitaoka, Y.; Aoki, D. Coexistence of Antiferromagnetism and Superconductivity near the Quantum Criticality of the Heavy-Fermion Compound $CeRhIn_5$. *Phys. Rev. B* **2003**, *90*, 077004-4.

(9) Si, Q.; Steglich, F. Heavy Fermions and Quantum Phase Transition. *Science (80-.).* **2010**, *329*, 1161–1167.

(10) Y. lsikawa , K. Mori a, K. Kamigaki a, T. Mizushima b, K. Oyabe b, S. U. b and K. S. b. The Dense Kondo Effect in Ternary Intermetallic Compounds Ce-Ni-Al. *J. Magn. Magn. Mater.* **1992**, *108*, 157–158.

(11) Onuki, Y. Magnetic Property of New Kondo Lattice Compound. *J. Phys. Soc. Jpn.* 1984, pp 1210–1213.

(12) Benbow, E. M.; Dalal, N. S.; Latturner, S. E. Spin Glass Behavior of Isolated , Geometrically Frustrated Tetrahedra of Iron Atoms in the Intermetallic $La_{21}Fe_8Sn_7C_{12}$. *J. Am. Chem. Soc.* **2009**, *131*, 3349–3354.

(13) Paulose, P. L.; Sampathkumaran, E. V.; Bitterlich, H.; Behr, G.; Löser, W. Anisotropic Spin-Glass-like and Quasi-One-Dimensional Magnetic Behavior in the Intermetallic Compound Tb_2PdSi_3. *Phys. Rev. B - Condens. Matter Mater. Phys.* **2003**, *67*, 1–4.

(14) Maple, M. B.; Smith, T. F. The Effect of Pressure on the Superconducting Transition Temperature of $La_{1-x}Ce_xAl_2$ and $La_{1-x}Gd_xAl_2$ Alloys. *Solid State Commun.* **1969**, *7*, 515–517.

(15) Clogston, A. M. Upper Limit for the Critical Field in Hard Superconductors. *Phys. Rev. Lett.* **1962**, *9*, 266–267.

(16) Felten, E. J. The Preparation of Aluminum Diboride, AlB_2. *J. Am. Chem. Soc.* **1956**, *78*, 5977–5978.

(17) Das, D. K.; Pitman, D. T. Preparation and Diffraction Data of Ba-AI Alloys. **1957**, *26*, 1175.

(18) Hoffmann, R.-D.; Pöttgen, R. AlB_2-Related Intermetallic Compounds – a Comprehensive View Based on Group-Subgroup Relations. *Zeitschrift für Krist. - Cryst. Mater.* **2001**, *216*, 127–145.

(19) Sarkar, S.; Peter, S. C. Structural Phase Transitions in a New Compound Eu_2AgGe_3. *Inorg. Chem.* **2013**, *52*, 9741–9748.

(20) Kwon, Y. U.; Corbett, J. D. Chemistry in Polar Intermetallic Compounds. The Interstitial Chemistry of Zr_5Sn_3. *Chem. Mater.* **1992**, *4*, 1348–1355.

(21) Zhao, J.-T.; Corbett, J. D. Zintl Phases in Alkali-Metal-Tin Systems: K_8Sn_{25} with Condensed Pentagonal Dodecahedra of Tin. Two A_8Sn_{44} Phases with a Defect Clathrate Structure. *Inorg. Chem.* **1994**, *33*, 5721–5726.

(22) Kauzlarich, S. M.; Brown, S. R.; Jeffrey Snyder, G. Zintl Phases for Thermoelectric Devices. *Dalt. Trans.* **2007**, No. 21, 2099.

(23) Graf, T.; Felser, C.; Parkin, S. S. P. Simple Rules for the Understanding of Heusler Compounds. *Prog. Solid State Chem.* **2011**, *39*, 1–50.

(24) Samson, S. The Crystal Structure of the Phase β Mg_2AI_3. *Acta Crystallogr.* **1965**, *19*, 401–413.

(25) Stiehler, M.; Rauchhaupt, J.; Giegengack, U.; Häussler, P. On Modifications of the Well-Known Hume-Rothery Rules: Amorphous Alloys as Model Systems. *J. Non. Cryst. Solids* **2007**, *353*, 1886–1891.

(26) Marakatti, V. S.; Peter, S. C. Synthetically Tuned Electronic and Geometrical Properties of Intermetallic Compounds as Effective Heterogeneous Catalysts. *Prog. Solid State Chem.* **2018**, *52*, 1–30.

(27) Peter, S. C.; Malliakas, C. D.; Kanatzidis, M. G. Structure and Unusual Magnetic Properties of $YbMn_{0.17}Si_{1.88}$. *Inorg. Chem.* **2013**, *52*, 4909–4915.

(28) Chondroudi, M.; Peter, S. C.; Malliakas, C. D.; Balasubramanian, M.; Li, Q.; Kanatzidis, M. G. $Yb_3AuGe_2In_3$: An Ordered Variant of the YbAuIn Structure Exhibiting Mixed-Valent Yb Behavior. *Inorg. Chem.* **2011**, *50*, 1184–1193.

(29) Kanatzidis, M. G.; Pöttgen, R.; Jeitschko, W. The Metal Flux: A Preparative Tool for the Exploration of Intermetallic Compounds. *Angew. Chemie Int. Ed.* **2005**, *44*, 6996–7023.

(30) Kittel, C. Introduction to Solid State Physics. *Wiley Student Ed.* **2018**, *2*, 43.

(31) Edwards, S. F.; Anderson, P. W. Theory of Spin Glasses. *J. Phys. F Met. Phys.* **1975**, *5*, 965–974. https://doi.org/10.1088/0305-4608/5/5/017.

(32) Mydosh, J. A. *Spin Glasses : An Experimental Introduction*; 1993.

(33) Mézard, M.; Parisi, G.; Sourlas, N.; Toulouse, G.; Virasoro, M. Replica Symmetry Breaking and the Nature of the Spin Glass Phase. *J. Phys.* **1984**, *45*, 843–854.

(34) Chevalier, B.; Pöttgen, R.; Darriet, B.; Gravereau, P.; Etourneau, J. Structural Chemistry and Magnetic Behaviour of the Ternary Silicides U_2TSi_3(T = Mn, Fe, Co, Ni, Ru, Rh, Pd, Os, Ir, Pt, Au). *J. Alloys Compd.* **1996**, *233*, 150–160.

(35) Keren, A.; Uemura, Y. J.; Luke, G.; Mendels, P.; Mekata, M.; Asano, T. Magnetic Dilution in the Geometrically Frustrated $SrCr_9pGa_{12-9}pO_{19}$ and the Roleof Local Dynamics: A Muon Spin Relaxation Study. *Phys. Rev. Lett.* **2000**, *84*, 3450–3453.

(36) Kondo, J. Resistance Minimum in Dilute Magnetic Alloys. *Prog. Theor. Phys.* **1964**, *32*, 37–49.

(37) Mathur, N. D.; Grosche, F. M.; Julian, S. R.; Walker, I. R.; Freye, D. M.;

Haselwimmer, R. K. W.; Lonzarich, G. G. Magnetically Mediated Superconductivity in Heavy Fermion Compounds. *Nature* **1998**, *394*, 39–43.

(38) Stewart, G. R. Heavy-Fermion Systems. *Mater. Sci. Technol. Diuision* **1979**, No. 1979.

(39) Taylor, P. Heavy-Fermion Intermetallic Compounds. *Contemp. Phys.* **2006**, *28* (1987), 143–157.

(40) Hundley, M. F.; Sarrao, J. L.; Thompson, J. D.; Movshovich, R.; Jaime, M. Unusual Kondo Behavior in the Indium-Rich Heavy-Fermion Antiferromagnet $Ce_3Pt_4In_{13}$. *Phys. Rev. B* **2001**, *65*, 1–7.

(41) Goodrich, R. G.; Harrison, N.; Teklu, A.; Young, D.; Fisk, Z. Development of the High-Field Heavy-Fermion Ground State in $Ce_xLa_{1-X}B_6$ Intermetallics. *Phys. Rev. Lett.* **1999**, *82*, 3669–3672.

(42) Fisk, Z.; Sarrao, J. L.; Smith, J. L.; Thompson, J. D. The Physics and Chemistry of Heavy Fermions. *Proc. Natl. Acad. Sci.* **1995**, *92*, 6663–6667.

Chapter 2

Structural Properties Relationship in a New Intermetallic Compound VNiSn

Chapter 2

Structural Properties Relationship in a New Intermetallic Compound VNiSn

2.1. Introduction

The Sc*T*Si (*T* = Fe, Co, Ni, Cu, Ru, Rh, Pd, Ir, Pt) silicide systems crystallize in the TiNiSi structure type with *Pnma* space group. Among them, ScFeSi[1], ScNiSi[2], ScCuSi[3], ScRhSi[4], and ScPtSi[5] have been studied by single crystal X-ray diffraction (XRD) and by solid-state NMR studies[6]. Depending on the size and valence electron concentration, the Sc*T*Sn stannides (*T* = Co, Ni, Cu, Pd, Ag, Pt, Au) crystallize in different structure types[7-11]. ScCoSn[12] and ScNiSn[13] adopt the orthorhombic TiNiSi type. ScCuSn and ScAuSn crystallize in LiGaGe and MgAgAs structure type, respectively[9,12]. ScPdSn[6], ScAgSn[10] and ScPtSn[6] crystallize with pronounced ZrNiAl type subcells, however, superstructures form due to the small size of the scandium atoms, i.e., the HfRhSn type[13] via doubling of the c axis for ScPdSn and ScPtSn[14] and the TiFeSi type[15] for ScAgSn[10]. The $Co_xNi_{1-x}MnGe$ compounds crystallize in the orthorhombic TiNiSi-type at low temperature and hexagonal Ni_2In type at high temperature[16].

The variation in atomic size and valance of the *T*NiSn (*T* = Ti, V, Cr, Mn, Fe, Co, Ni, Cu) series are expected to show some change in the crystal structure mostly evolution of new structure types. TiNiSn exists in the MgAgAs type[17], which is a non-centrosymmetric cubic structure (space group *F*-43*m*). MgAgAs is a ternary ordered variant of the CaF_2 structure and can be derived from the tetrahedral ZnS-type structure by filling the octahedral lattice sites. A characteristic feature of this half-Heusler structure type is the presence of three interpenetrating FCC sub-lattices, each of which are occupied by the Ti, Ni and Sn atoms. The corresponding occupied Wyckoff positions are 4*a* (0, 0, 0), 4*b* (1/2, 1/2, 1/2), and 4*c* (1/4, 1/4,1/4), respectively. Surprisingly, *T*NiSn (*T* = V, Cr, Mn) compounds are not reported till date. On the other hand, in the second half of 3d series, FeNiSn, and CoNiSn are reported in the AlB_2 type structure (space group $P6_3/mmc$)[18-19].

Here, in this work we are reporting VNiSn a new intermetallic. Our detailed single crystal XRD analysis revealed that VNiSn crystallizes the AlB_2 structure type. VNiSn is

characterized by resistivity, SEM, magnetic, mössbauer, XANES and electronic band structure.

2.2. Experimental Section

2.2.1 Synthesis

The following elements were used as purchased from Alfa-Aesar without any further purification: V (chunk, 99.99%), Ni (wire, 99.999%) and Sn (shots, 99.999%). The VNiSn compound was prepared by arc-melting of these metals in an stochiometric ratio (total weight of reactant was ~250 mg) in an argon atmosphere using a non-consumable tungsten electrode and a water-cooled copper hearth. The compound was melted by the Arc melter for one time and the mass of which had been determined carefully, were controlled after melting for mass loss. The mass loss was less than 2%.

2.2.2 Powder X-ray diffraction (XRD) - Phase identity and purity of the VNiSn and 2% Ti doped VNiSn compound was determined by powder XRD experiments (**Figure 2.1**) that were carried out on a Bruker D8 Discover diffractometer using Cu Kα radiation (λ = 1.5406 Å) and calibrated against corundum standard, over the angular range $10° \leq 2\theta \leq 90°$, with a step size of 0.02° at 298 K.

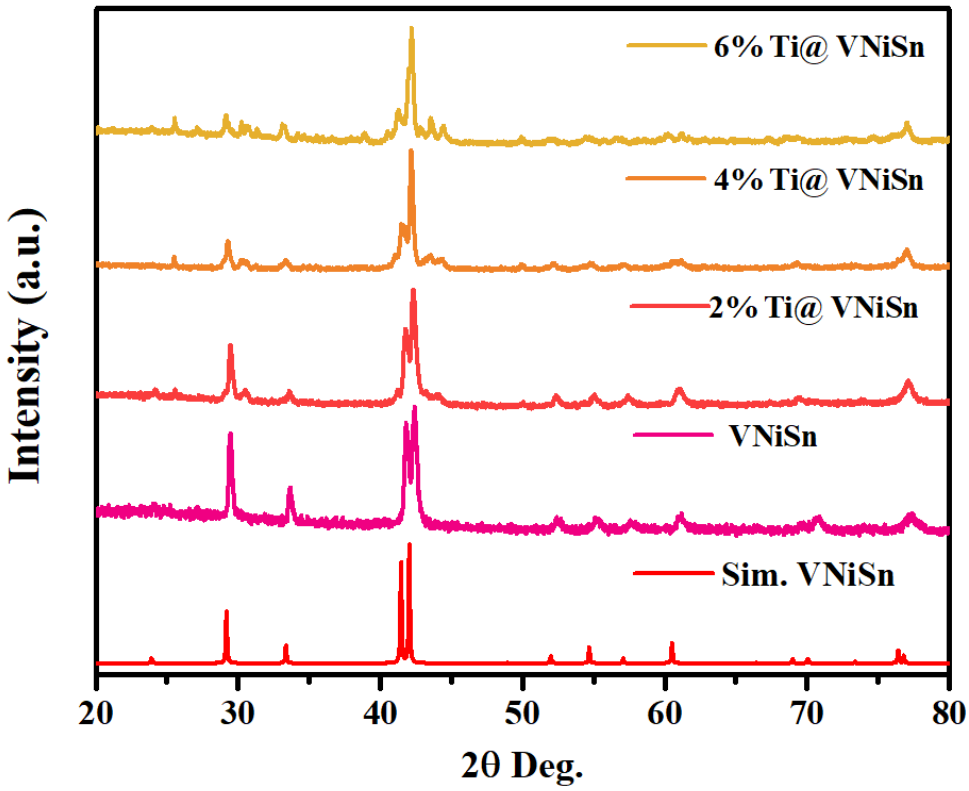

Figure 2.1. Powder XRD of various percentage of Ti@ VNiSn with simulated pattern of VNiSn obtained from single crystal XRD.

2.2.3 Field Emission Scanning Electron Microscopy (FE-SEM)-Energy Dispersive X-ray Spectroscopy (EDS)

Semi quantitative microanalyses were performed on VNiSn single crystals using a Leica 220i electron microscope (SEM) equipped with Bruker 129eV energy dispersive X-ray analyzer (EDS). Data were acquired with an accelerating voltage of 20kV and 90s accumulation time. The EDS analysis performed on VNiSn compound, percent showed the atomic composition for VNiSn is 1:1:1. The EDS spectrum is shown in **Figure 2.2b**. The values are in accordance to the ones obtained from the refinement of single crystal XRD data. Field emission scanning electron microscopy (FE-SEM) image of VNiSn single crystal is shown in **Figure 2.2a.**

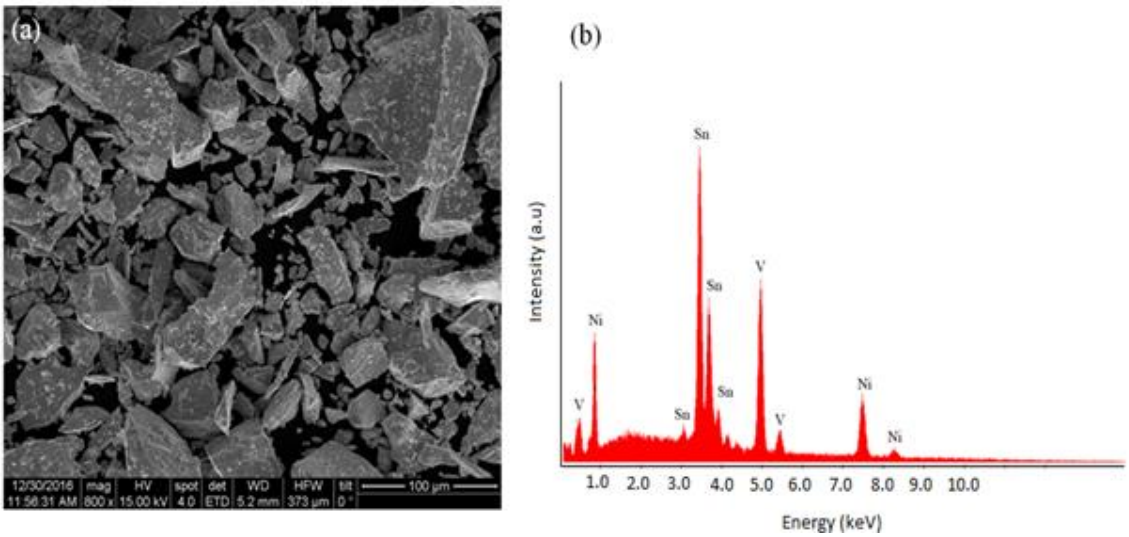

Figure 2.2. (a). FESEM image and (b). EDS spectrum of VNiSn.

2.2.4 Single crystal XRD

Single crystal X-ray diffraction data were collected on a Bruker Smart X2 APEX II CCD diffractometer having a normal focus, 2.4 kW sealed tube X-ray source with graphite monochromatic Mo-Kα radiation (λ = 0.71073 Å) operating at 50 kV and 30 mA, with ω scan mode. Suitable single crystal of the VNiSn compound was mounted on a thin glass (~0.1 mm) fibre with commercially available super glue. The programme SAINT was used for integration of diffraction profiles and absorption correction was made with SADABS programme.

The crystal structure of VNiSn was solved by SHELXS 97[20] and refined by a full matrix least-squares method using SHELXL with anisotropic atomic displacement parameters for all atoms. As a check for the correct composition, the occupancy parameters were refined in a separate series of least-squares cycles. The crystallographic

details of the reported CoNiSn compound were taken at the initial step of the refinement. All bond lengths are within the acceptable range. Packing diagrams were generated with Diamond. The data collection and structure refinement are listed in **Table 2.1**. The standard atomic positions and isotropic atomic displacement parameters and the anisotropic displacement parameters are listed in **Tables 2.2 and 2.3** respectively.

2.2.5 Magnetic measurements

Magnetic measurements were performed on single phase polycrystalline VNiSn and 2% Ti doped VNiSn sample using Quantum design superconducting quantum interference device (QD-SQUID) magnetic property measurement system (MPMS). Magnetic susceptibility of VNiSn was measured in zero field cooled (ZFC) and field cooled (FC) an applied field of 1000 Oe as a function of temperature. Field dependent magnetization measurements were also carried out at selected temperatures as a function of applied magnetic field.

Table 2.1. Crystal data and structure refinement for VNiSn at 296(2) K.

Empirical formula	VNiSn
Formula weight	228.34
Wavelength	0.71073 Å
Crystal system	Hexagonal
Space group	$P6_3/mmc$
Unit cell dimensions	a = 4.2956(10) Å, α = 90° b = 4.2956(10) Å, β = 90° c = 5.3680(17) Å, γ = 120°
Volume, Z	85.78(5) $Å^{3,}$ 1
Density (calculated)	4.420 g/cm^3
Absorption coefficient	15.015 mm^{-1}
F(000)	101
Crystal size	0.1x 0.12x 0.2 mm^3
θ range for data collection	5.482 to 29.568°
Index ranges	-5<=h<=5, -5<=k<=5, -7<=l<=5
Reflections collected	971
Independent reflections	60 [R_{int} = 0.3544]
Completeness to θ = 25.242°	97.6%
Refinement method	Full-matrix least-squares on F^2
Data / restraints / parameters	60 / 0 / 10
Goodness-of-fit	0.975
Final R indices [I > 2σ(I)]	R_{obs} = 0.0580, wR_{obs} = 0.1267
R indices [all data]	R_{all} = 0.0971, wR_{all} = 0.1357
Extinction coefficient	0.006(16)
Largest diff. peak and hole	2.422 and -1.427 e·Å^{-3}

$R = \Sigma||F_o|-|F_c|| / \Sigma|F_o|$, $wR = \{\Sigma[w(|F_o|^2 - |F_c|^2)^2] / \Sigma[w(|F_o|^4)]\}^{1/2}$ and $w=1/[\sigma^2(Fo^2)+(0.0551P)^2]$ where $P=(Fo^2+2Fc^2)/3$

Table 2.2. Atomic coordinates ($x10^4$) and equivalent isotropic displacement parameters ($Å^2x10^3$) for VNiSn at 296(2) K with estimated standard deviations in parentheses.

Label	*X*	*Y*	*Z*	Occupancy	U_{eq}^*
Sn	3333	6666	2500	1	47(2)
V	3333	6666	7500	0.82(5)	62(7)
Ni	0	0	0	0.93(2)	32(3)

*U_{eq} is defined as one third of the trace of the orthogonalized U_{ij} tensor.

Table 2.3. Anisotropic displacement parameters ($Å^2x10^3$) for VNiSn at 296(2) K with estimated standard deviations in parentheses.

Label	U_{11}	U_{22}	U_{33}	U_{12}	U_{13}	U_{23}
Sn	18(3)	18(3)	26(2)	29(2)	0	0
V	10(9)	10(9)	47(9)	35(5)	0	0
Ni	35(3)	35(3)	24(4)	18(2)	0	0

The anisotropic displacement factor exponent takes the form: $-2\pi^2[h^2a^{*2}U_{11} + ... + 2hka^*b^*U_{12}]$.

2.2.6 Electrical Resistivity

Resistivity measurements performed on polycrystalline samples of VNiSn over the temperature range of 7.5−300 K using a four-probe dc technique having contacts made with silver paste. Measurements were conducted using Labview program, Keithley 2400 C and Lakeshore 336 temperature controller.

2.2.7 X-ray absorption near edge spectroscopy (XANES)

X-ray absorption near edge spectroscopy (XANES) experiments at room temperature on VNiSn was performed at PETRA III, P06 beamline of DESY, Germany. Measurements at the V K edge and Ni K edge at ambient pressure were performed in transmission mode using gas ionization chambers to monitor the incident and transmitted X-ray intensities. Monochromatic X-rays were obtained using a Si (111) double crystal monochromator which was calibrated. The beam was focused employing a Kirkpatrick–Baez (K–B) mirror optic. A rhodium coated X-ray mirror was used to suppress higher order harmonics. A CCD detector was used to record the transmitted signals. The sample was prepared by mixing an appropriate amount of finely ground powder with cellulose and cold pressing them to a pellet.

2.2.8 ^{119}Sn Mössbauer Spectroscopy

A $Ca^{119}SnO_3$ was used as source for ^{119}Sn Mössbauer spectroscopy. All the polycrystalline samples were placed in sample holder made up of polyacrylate.

Measurements were done on recoil velocity of 8.004 mm/s under transmission geometry at 298 K with total counting time of 47 hours.

2.2.9 Computational Details

All the calculations were carried out using Dmol^3 program. GGA-PBE functional was used to describe the electronic exchange and correlation effects. DNP is chosen as the basis set with orbital cut-off of 4.4 Å. The convergence threshold values for energies, force and displacement are specified as 2 x 10^{-5} Ha, 4 x 10^{-3} Ha/Å, 5 x 10^{-3} Å, respectively, while the SCF convergence threshold is 1 x 10^{-5} Ha. Electron thermal smearing value of 0.005 Ha is employed for all the calculations to enhance SCF convergence efficiency.

2.3 Results and Discussions

2.3.1 Reaction Chemistry

The VNiSn compound was obtained from the arc-melting technique is stable in air and no decomposition observed even after few days. The experimental PXRD pattern compared with the simulated pattern obtained from SCXRD data (**Figure 2.1**) and found to match well with the SCXRD data.

2.3.2 Crystal structure

The crystal structure of VNiSn in ab projection is shown in **Figure 2.4.** The VNiSn compound crystallize in hexagonal BeZrSi[21] structure type, a ternary variant of the AlB_2 type[22] with $P6_3/mmc$ space group and lattice parameters are, $a = b = 4.2956(10)$ Å and c = 5.3688(17) Å.

The crystal structure of VNiSn ($P6_3/mmc$) can be related to the AlB_2 structure ($P6/mmm$) by using group-subgroup relation. In the AlB_2 structure, B atoms form the hexagonal sheet-like graphite while Al atoms occupy the corner of unit cell. In VNiSn, Ni atoms replace Al. Alternatively V and Sn atoms formed hexagonal slabs stacked of V_3Sn_3 along the *c*-axis. These V_3Sn_3 layers are rotated 60^0 in c-direction and Ni atoms sandwiched between the planes as seen in **Figure 2.3**. This results in doubling of *c*-axis. Due to two different atoms in planar sheet there is a loss of inversion centre resulting reduction in few symmetries. This symmetry reduction leads to a reduction of half of the inversion centre, half of the translations and half of the symmetry axis perpendicular to *c*-direction. This symmetry reduction also causes the glide plane c instead of mirror plane perpendicular to [210] along with splitting of the 2*d* Wyckoff position of B atom into two symmetry-independent position 2*c* and 2*d* occupied by Sn and V atoms, respectively. This group-subgroup relation can be seen in the **Figure 2.3.**

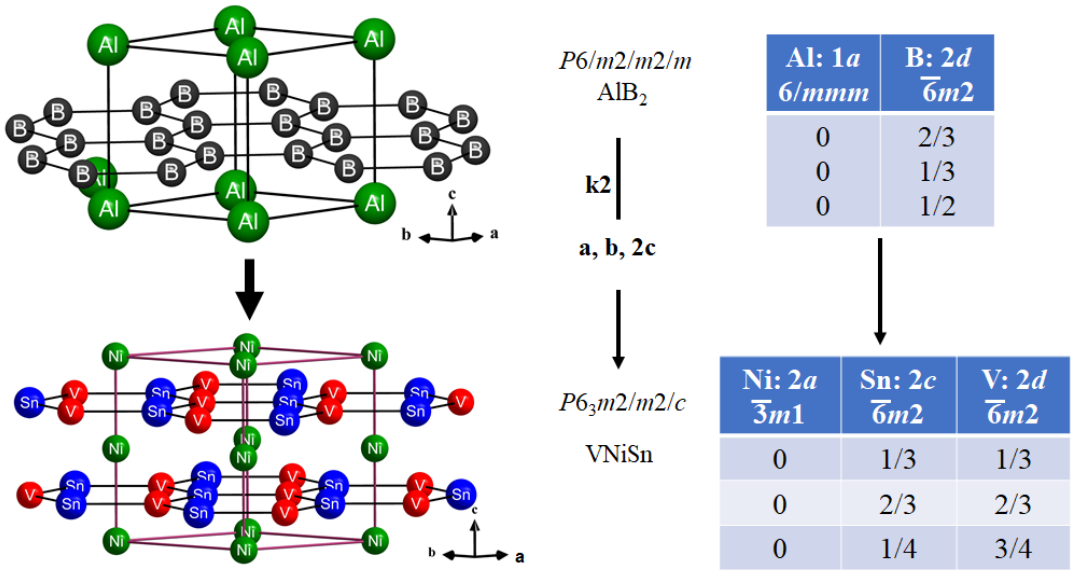

Al: 1*a* 6/*mmm*	B: 2*d* $\bar{6}m2$
0	2/3
0	1/3
0	1/2

Ni: 2*a* $\bar{3}m1$	Sn: 2*c* $\bar{6}m2$	V: 2*d* $\bar{6}m2$
0	1/3	1/3
0	2/3	2/3
0	1/4	3/4

Figure 2.3. (a) Structure relation between AlB_2 and VNiSn. **(b)** Group-subgroup relation of AlB_2 and VNiSn. Due to doubling of *c*-axis the z co-ordinate is halved. Index of symmetry reduction is 2.

In general, the equiatomic intermetallic compounds *XYZ* (*X* = alkaline earth/early transition metal, *Y* = early/late transition metal element, *Z* = main group element) crystallize in the structure types related to the AlB_2 family. The ordered superstructures of this composition crystallize in the LiGaGe[23], NdPtSb[24], and ZrBeSi[21] type structures. The late transition metals and the main group elements form Y_3Z_3 hexagons, which are connected in a 2-dimensional honeycomb network. Disorder between the transition metals and the main group elements leads to the pseudo-binary structure types like Ni_2In, or $CaIn_2$.

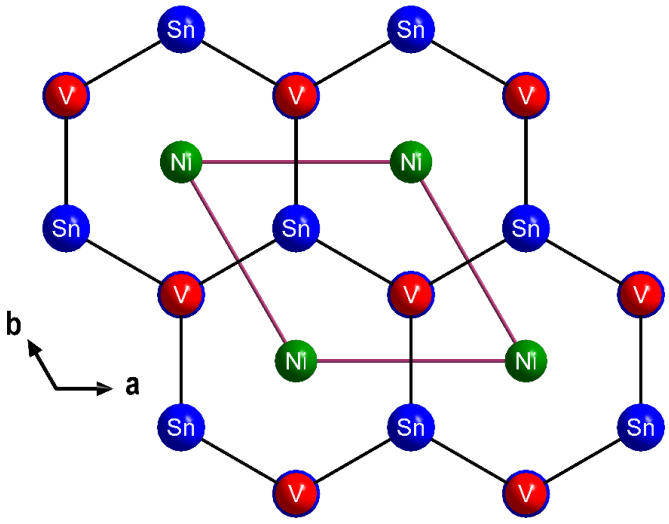

Figure 2.4. Crystal structure of VNiSn projected onto *ab* plane.

The hexagon layers can be planar like in graphite (found in the ZrBeSi and AlB_2 types), weakly puckered (NdPtSb type) or strongly puckered with short interatomic distances between the layers leading to a wurtzite-related structure with a 3-dimensional network (LiGaGe type). Compared to the compounds with the stuffed zinc blende structure, namely the *C*1*b* half-Heusler compounds, the LiGaGe structure type which is the focus of this contribution has a free lattice parameter, the *c*/*a* ratio, which should be 1.633 for the ideal hexagonal *wurtzite* structure. Beside the variable *c*/*a* ratio, the free *z* parameter of the 2*b* positions allows different degrees of puckering of the hexagons leading to structures that can vary almost continuously from three dimensional to quasi-two dimensional. Due to this reduction in symmetry in comparison with the half-Heusler compounds, a large variety of different structure types are possible as described above. The different superstructures are related via group-subgroup relations as recently reviewed[25]. The bonding features in such materials have been discussed in several overview[26].

The coordination environment of V, Ni and Sn atoms are shown in **Figure 2.5a-c**. The V and Sn atoms are situated in a pentacapped trigonal prism made up of Ni_6Sn_5 and V_5Ni_6 respectively. The Ni atom has 14-coordinate environment having six Sn atoms, six V and two Ni atoms which is bicapped hexagonal prism made up of $V_6Ni_2Sn_6$.

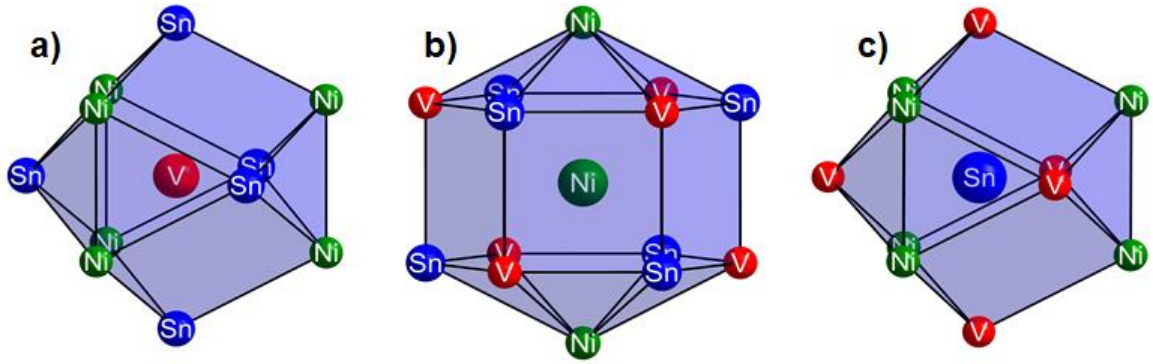

Figure 2.5. a) Coordination environment of (a) Vanadium (b) Nickel (c) Tin in VNiSn.

2.3.3 X-ray absorption near edge spectroscopy (XANES)

To confirm the oxidation state of V and Ni, we have performed the XANES measurements, which is a strong experimental tool to firmly establish the valence state of an element in a compound. A signal at 5483.01 eV was observed in the V-K_{edge} X-ray absorption spectrum of VNiSn (**Figure 2.6**). This value is characteristic of vanadium zero oxidation state configuration, which is confirmed in the magnetic susceptibility data

(discussed below). There is an absence of white line in XANES spectrum was observed for Ni $K_{edge,}$ which is indicating nickel is in zero oxidization state.

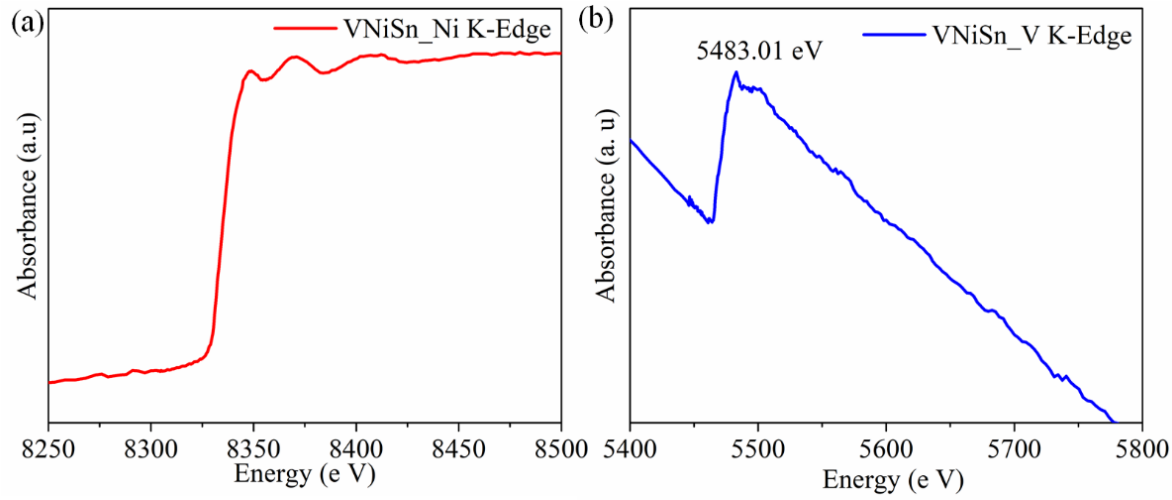

Figure 2.6. Ni K-absorption edge and V K- absorption edge XANES spectrum for VNiSn compound.

2.3.5 Ti substituted on VNiSn

TiNiSn a well-studied thermoelectric material crystallise in cubic structure type in space group *Fm*-3*m* but VNiSn crystallises in hexagonal structure type. This is surprising that with V inclusion the lattice symmetry got decreased to hexagonal. To enquire this we had done the substation of V with Ti atoms to see the structural transformation from hexagonal to cubic structure type.

We had done profile fitting using FULLPROF on $V_xTi_{1-x}NiSn$ (x = 0, 0.2, 0.4, 0.6) We observed one anomaly from the powder XRD plot of Ti doped VNiSn in **Figure 2.1**. In general, upon doping of element having larger atomic size than the parent element leads to a shift of peak position to the lower angle in powder XRD pattern consequently leads to increasing in lattice parameter of parent system. Refinement plot is given in **(Figure 2.7)** and the lattice parameters were compared with VNiSn lattice parameter obtained from Single crystal XRD, are given in the **Table 2.4**.

Table 2.4. Comparison of the lattice parameters of $V_xTi_{1-x}NiSn$ (x = 0, 0.2, 0.4, 0.6) obtained from Single Crystal XRD.

Compound	a = b (Å)	c (Å)
VNiSn	4.2956	5.3680
$V_{0.98}Ti_{0.2}NiSn$	4.2456	5.3752
$V_{0.96}Ti_{0.4}NiSn$	4.2864	5.3706
$V_{0.94}Ti_{0.6}NiSn$	4.2934	5.4210

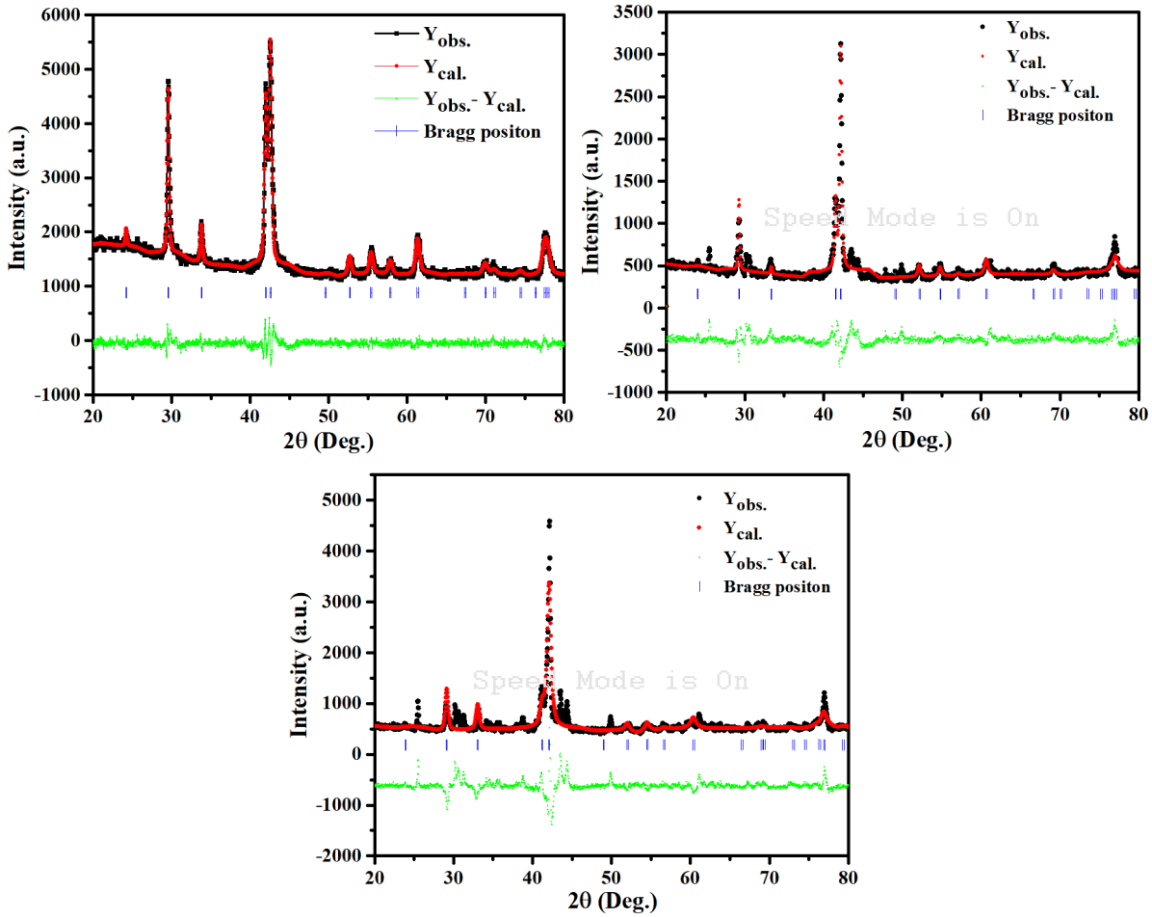

Figure 2.7. Profile fitting for Ti substitution on $V_xTi_{1-x}NiSn$ (x = 0, 0.2, 0.4, 0.6)

So, from the **Table 2.4**, for $V_{0.96}Ti_{0.4}NiSn$ and $V_{0.94}Ti_{0.6}NiSn$ *a* and *b* lattice parameter are slightly decreased but *c* lattice parameter is increased by substantial amount in the case of $V_{0.94}Ti_{0.6}NiSn$. This can be attributed to the substitution of Ti atom at vanadium sites. Due to large size of Ti atoms, it is not able to occupy into the V_3Sn_3 plane and compressing *a-b* lattice parameter while increasing the *c* parameter. Effect of $V_xTi_{1-x}NiSn$ is also evident form Mossbauer spectroscopic measurements, which is discussed below.

2.3.5 Mössbauer spectroscopy

The room temperature Mössbauer spectra are shown in **Figure 2.8**. All the data was fitting using Lorentzian model (area equal method) and were best fitted with one signal, which is in consistent with the crystal structure. The fitting parameters are listed in **Table 2.5**. All single signal lines in spectra showing there is only one type of Sn atom is present which is also supported from our single crystal data as well as theoretical calculation. The isomer shifts in VNiSn and other $V_xTi_{1-x}NiSn$ systems is in the range of

1.4679-1.6158 which is in the typical range of related stannides[27]. A very slight isomers shift from pure VNiSn showing there is approximately no change in oxidation state of Sn upon Ti substitution, which is slightly positive as evident from the theoretical calculations. However, in case of $V_{0.96}Ti_{0.4}NiSn$ and $V_{0.94}Ti_{0.6}NiSn$ isomer shift is lowering by 0.1143 mm/s indicating lesser electron density at Sn nucleus. This decrease in electron density at nucleus can be understood from the Ti atom occupying the V_3Sn_3 plane and slight electropositive nature of Ti atom than V decreasing s-electron density at Sn.

Electric quadrupole splitting indicating non-cubic geometry of Sn coordination. Quadrupole splitting value close to one showing the low site symmetry of Sn atoms (Wyckoff position is 2*c*)[41]. $V_{0.98}Ti_{0.2}NiSn$ increases the site symmetry evident form almost equal intensity of fitted signal while upon increasing the Ti concentration, Sn site symmetry got decreased. Sn showing the slight positive nature which also confirmed from theoretical charge distribution calculation.

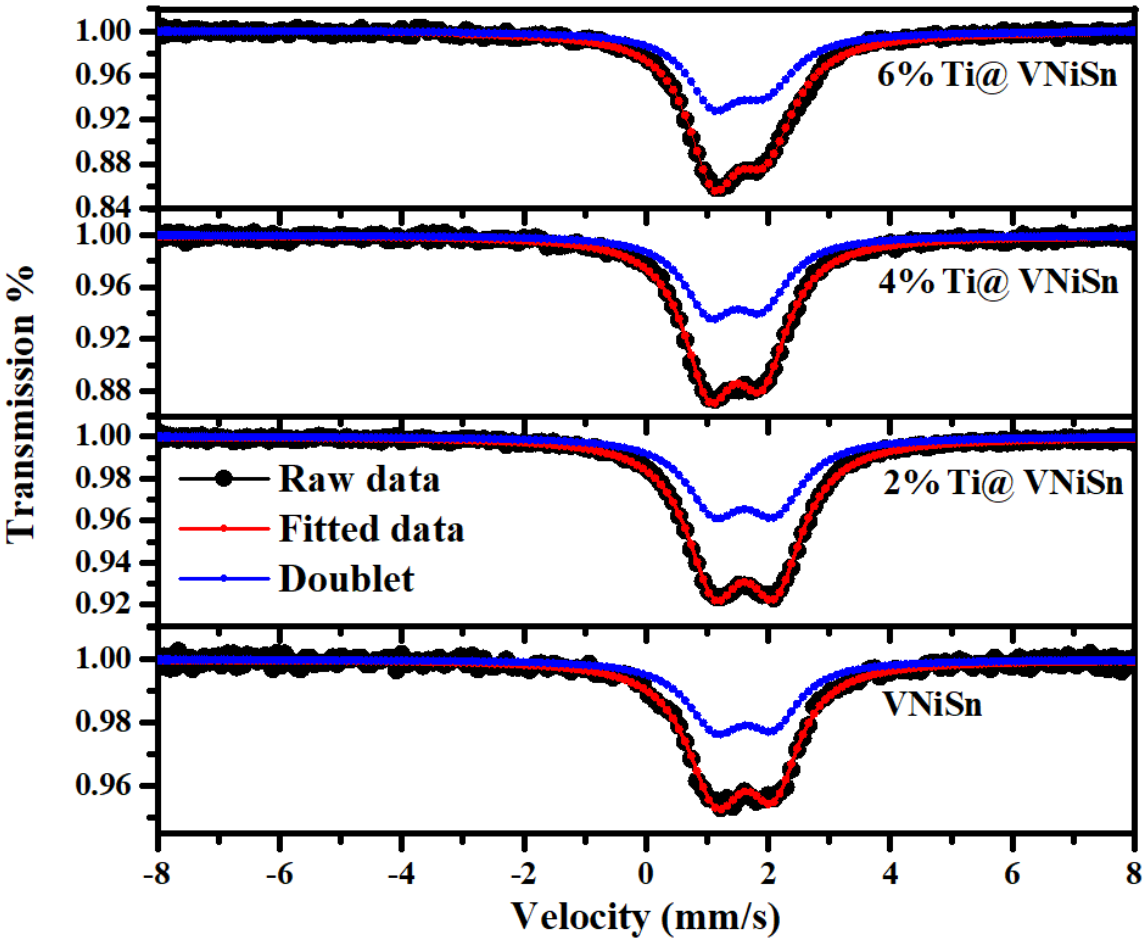

Figure 2.8. Mössbauer spectra of various percentage of Ti@VNiSn at room temperature

Table 2.5. Fitting parameters of ^{119}Sn Mössbauer spectroscopic measurements of VNiSn and δ, isomer shift; ΔE_Q, electric quadrupole splitting; Γ, experimental line width.

Compound	δ (mm/s)	Γ (mm/s)	ΔE_Q (mm/s)	Area 2:1	χ^2
VNiSn	1.5816	1.0087	-0.9476	1.2833	1.145
$V_{0.98}Ti_{0.2}NiSn$	1.6158	1.0969	-0.9938	1.1037	1.345
$V_{0.96}Ti_{0.4}NiSn$	1.4673	1.0368	-0.8655	1.0626	1.359
$V_{0.94}Ti_{0.6}NiSn$	1.5272	1.1651	-0.85098	1.0338	1.845

2.3.6 Theoretical calculations – Electronic band structure and partial density of states for VNiSn are plotted in **Figure 2.9a** and **2.9b**, respectively. Bands at K, G, M symmetry point are crossing the fermi level (**Figure 2.9a)** and there is substantial amount of density of states at fermi level **Figure (2.9b).** It shows that VNiSn is metallic nature, which is confirmed experimentally by resistivity measurement. At Fermi level the major contribution to density of states comes from d-orbitals.

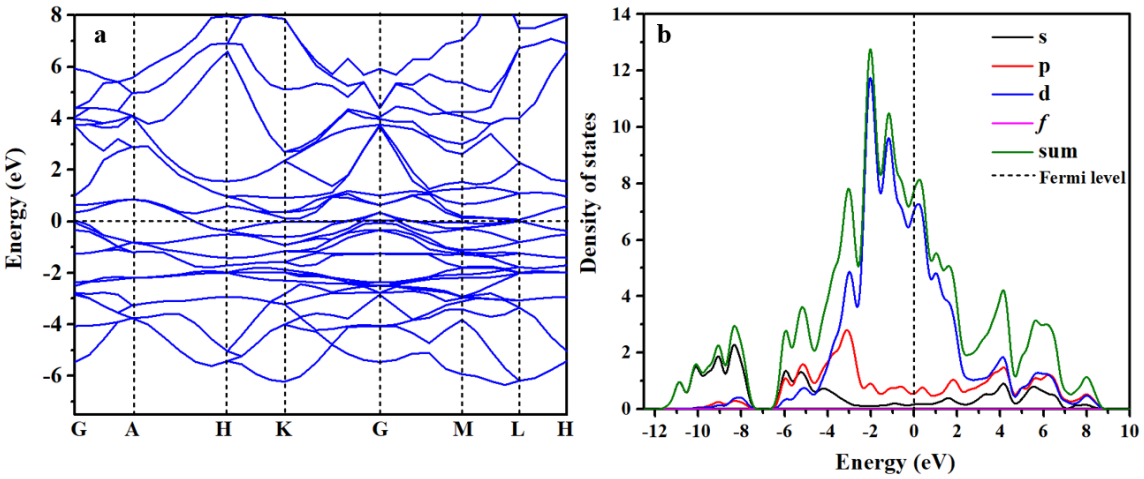

Figure 2.9. Density functional theory (DFT) calculation on VNiSn. a) Electronic band structure of VNiSn showing metallic behaviour, b) Density of states and partial density of states.

2.3.7. Physical Properties

2.3.7.1. Magnetism

The magnetic properties of VNiSn were measured on polycrystalline samples within the temperature range 2-300 K. The magnetic susceptibility data of VNiSn compound is plotted in **Figure 2.10a.** Magnetic susceptibility data showing the

paramagnetic nature of the sample. Susceptibility increases at low temperature, which is reminiscent of spin ordering. The nickel atom is in zero oxidation state so it's not contributing for the effective magnetic moment. We have observed bi-furcation between field-cooled and zero-field cooled data at higher temperature. Magnetization of the compound VNiSn was measured as a function of ramping field at temperatures 2 and 300 K in the applied magnetic field range of ±60 kOe (shown in **Figure 2.10c-d**). The magnetic moment is not saturating at the highest applied field. The curves at 2 K and 300 K showed a hysteresis loop at lower applied magnetic field and it is linear at higher applied magnetic field indicates the weak ferromagnetic state of the sample. This may be due to unreacted Ni present in the sample.

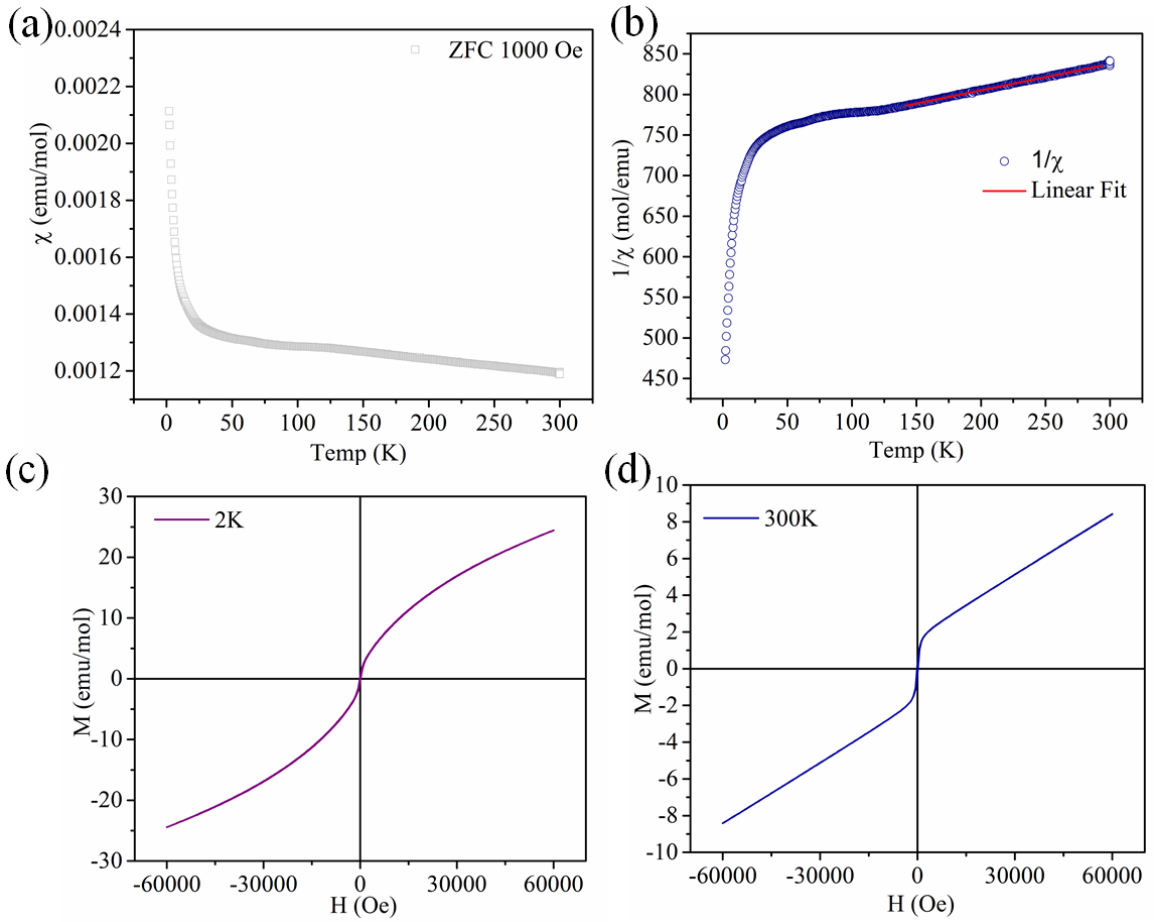

Figure 2.10. (a) Temperature dependence of molar susceptibility in ZFC mode, (b) inverse molar susceptibility of VNiSn at 1000 Oe applied magnetic field. (c-d) Magnetization measured as a function of magnetic field at T = 2 K and 300 K for VNiSn.

2.3.7.2. Electrical resistivity

Temperature dependence of DC resistance measurement was carried out using a standard linear four probe method through ARS cryostat for the temperature ranges between 300 and 7.5 K. **Figure 2.11a** depicts resistance vs. temperature results for VNiSn

measured in cooling and warming processes while applying an excitation current value of 1 mA between two inner probes. It clearly shows a strong metallic behaviour through entire temperature range. At a low-temperature range of 0-10 K, the $\rho(T)$ data can be fitted to the power law function, $\rho = \rho_0 + AT^n$, where ρ_0 is the residual resistivity expressed in units of Ωcm, A and *n* are the fitting parameters. The values obtained from the fit are shown in **Figures 2.11b**. According to Fermi-liquid theory, at low temperatures, the resistivity varies as $\rho = \rho_0 + AT^2$. It has been observed experimentally, when electron-electron scattering dominates over electron-phonon scattering, $\rho \alpha T^2$. The value obtained from the fit power is close to 2 which clearly indicate that the system exhibiting Fermi liquid state. The residual resistivity (ρ_0) for VNiSn system is 0.0182 Ω.cm.

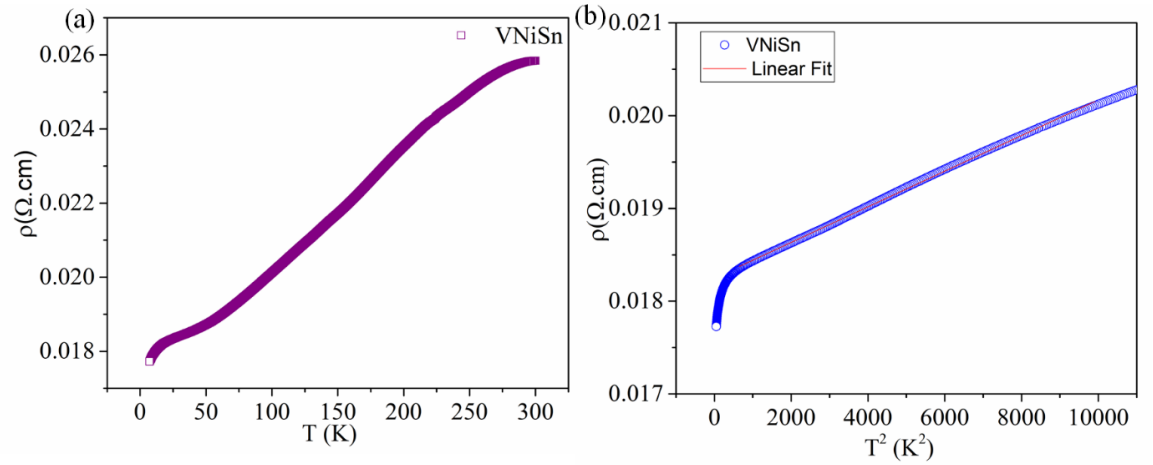

Figure 2.11. (a) Temperature dependence of resistivity for VNiSn and (b) The low temperature data has been fitted to the power law, $\rho = \rho_0 + AT^n$.

2.4. Conclusion

One of the biggest challenges in the field of intermetallic chemistry is the synthesis and crystal growth of unknown compounds. We have successfully synthesized a new compound VNiSn using the arc-melting technique, which is an ordered compound of the AlB_2 type. The magnetic measurement reveals that VNiSn is paramagnetic in nature and the resistivity data suggest metallic nature with Fermi-liquid behaviour. We are trying to understand the change in crystal structure from AlB_2 to Half-Heusler upon substitution in which we successfully doped till 6%.

References

(1) Bodak, O. Y.; Kotur, B. Y.; Gladushevskij, J. Y. The Scandium-Nickel-Silicon System. *Dopov. Akad. Nauk. Ukr. RSR., Ser. A* **1976**, *7*, 655–657.

(2) On, A. N.; Crystal, T. H. E.; Two, O. F. ScCuSi Phases. *J. Less-Common Met.* **1981**, *81*, 71–78.

(3) Bergstein, A.; Kleinert, P. Partial Phase Diagram of the System $Mn_xFe_{3-X}Oy$. *Collect. Czechoslov. Chem. Commun.* **1964**, *29*, 2549–2551.

(4) Hovestreydt, E.; Engel, N.; Klepp, K.; Parthg, E. Quai Ernest-. *J. Less-Common Met.* **1982**, *85*, 247–274.

(5) Harmening, T.; Eckert, H.; Fehse, C. M.; Sebastian, C. P.; Pöttgen, R. ^{45}Sc Solid State NMR Studies of the Silicides ScTSi (T=Co, Ni, Cu, Ru, Rh, Pd, Ir, Pt). *J. Solid State Chem.* **2011**, *184*, 3303–3309.

(6) Dwight, A. E.; Harper, W. C.; Kimball, C. W. HoPtSn and Other Intermetallic Type Structure Compounds with the Fe_2P- Type Structure. *J. Less-Common Met.* **1973**, *30*, 1–8.

(7) Larson, P.; Mahanti, S. D.; Kanatzidis, M. G. Structural Stability of Ni-Containing Half-Heusler Compounds. *Phys. Rev. B - Condens. Matter Mater. Phys.* **2000**, *62*, 12754–12762.

(8) Derkach, V. A.; Kotur, B. Y.; Gorelenko, Y. K.; Skolozdra, R. V. Magnetic Properties of $ScCo_2Sn$-ScCoSn Alloys. *Inorg. Mater.* **1997**, *33*, 814–816.

(9) Sebastian, C. P.; Eckert, H.; Rayaprol, S.; Hoffmann, R. D.; Pöttgen, R. Crystal Chemistry and Spectroscopic Properties of ScAuSn, YAuSn, and LuAuSn. *Solid State Sci.* **2006**, *8*, 560–566.

(10) Sebastian, C. P.; Zhang, L.; Fehse, C.; Hoffmann, R. D.; Eckert, H.; Pöttgen, R. New Stannide ScAgSn: Determination of the Superstructure via Two-Dimensional ^{45}Sc Solid State NMR. *Inorg. Chem.* **2007**, *46*, 771–779.

(11) Kotur, B. Y.; Klyuchka, I. P. New Ternary Stannides of Scandium and Cobalt (Nickel Copper). *Inorg. Mater.* **1989**, *25* (4), 597–599.

(12) Sebastian, C. P.; Fehse, C.; Eckert, H.; Hoffmann, R. D.; Pöttgen, R. Structure,119Sn Solid State NMR and Mössbauer Spectroscopy of *RE*CuSn (*RE* = Sc, Y, La, Lu). *Solid State Sci.* **2006**, *8*, 1386–1392.

(13) Zumdick, M. F.; Poettgen, R. Determination of the Superstructures for the Stannides ZrIrSn, HfCoSn, and HfRhSn. *Zeitschrift fuer Krist.* **1999**, *214*, 90–97.

(14) M, R.; Pöttgen, R.; H, R.; Trillb, H.; M, B. D.; Piotrow, H.; Zum, M. F. - Structure Refinements and 119Sn Mössbauer Spectroscopy. *B Chem. Sci.* **2001**, *56*, 589–597.

(15) Jeitschko, W. The Crystal Structure of MoCoB and Related Compounds. *Acta Crystallogr. Sect. B Struct. Crystallogr. Cryst. Chem.* **1968**, *B24*, 815–822.

(16) Güçlü, F.; Özdemir, A.; Dubenko, I.; Samanta, T.; Ali, N.; Kervan, N.; Kervan, S. Magnetic Properties of the $FeMn_{1-X}Ni_xGe$ Compounds. *J. Magn. Magn. Mater.* **2013**, *327*, 7–10.

(17) Jeitschko, W. Transition Metal Stannides with MgAgAs and $MnCu_2Al$ Type Structure. *Metall. Trans.* **1970**, *1*, 3159–3162.

(18) Castelliz, L. Kristallstruktur von Mn_5Ge_3 Und Einiger Ternärer Phasen Mit Zwei Übergangselementen. *Monatshefte für Chemie und verwandte Teile anderer Wissenschaften* **1953**, *84*, 765–776.

(19) Buschow, K. H. J.; van Engen, P. G.; Jongebreur, R. Magneto-Optical Properties of Metallic Ferromagnetic Materials. *J. Magn. Magn. Mater.* **1983**, *38*, 1–22.

(20) Sheldrick, G. M. Crystal Structure Refinement with SHELXL. *Acta Crystallogr. Sect. C Struct. Chem.* **2014**, *71*, 3–8.

(21) Nielsen, J. W.; Baenziger, N. C. The Crystal Structures of ZrBeSi and ZrBe 2. *Acta Crystallogr.* **1954**, *7*, 132–133.

(22) Felten, E. J. The Preparation of Aluminum Diboride, AlB. *J. Am. Chem. Soc.* **1956**, *78*, 5977–5978.

(23) Schuster, H. TernSre Phasen Im Dreistoffsystem in Einem Grol3eren Teilgebiet Dieses Dreistoffsystems Durchgefuhrt . **1974**, *240*, 233–240.

(24) Wenski, G.; Mewis, A. *RE*PtX Compounds with Structures Related to $A1B_2$ and MgAgAs-Type (*RE* = Y, Rare Earth Element; *X* = P, As, Sb). *Zeitschrift fur Krist. - New Cryst. Struct.* **1986**, *176*, 125–134.

(25) Hoffmann, R.-D.; Pöttgen, R. AlB_2-Related Intermetallic Compounds-a Comprehensive View Based on Group-Subgroup Relations. **2001**, *216*, 127–145.

(26) Pöttgen, R.; Borrmann, H.; Felser, C.; Jepsen, O.; Henn, R.; Kremer, R. K.; Simon, A. Crystal and Electronic Structures of ScAuGe, CeAuGe, and LuAuGe: A Transition from Two- to Three-Dimensional [AuGe] Polyanions. *J. Alloys Compd.* **1996**, *235*, 170–175.

(27) Lees, J. K.; Flinn, P. A. Mössbauer Effect in Tin Compounds: Interpretation of Isomer Shifts and Determination of the Nuclear Radius Change In ^{112}Sn. *J. Chem. Phys.* **1968**, *48* (2), 882.

Chapter 3

Room temperature ferromagnetism in a probable Kondo material $Yb_2Co_{1-x}In_{3+x}$

Chapter 3

Room temperature ferromagnetism in a probable Kondo material $Yb_2Co_{1-x}In_{3+x}$

3.1 Introduction

Rare-earth (*RE*) based compounds are fascinating due to the presence of strongly localized *f*-electrons that induces different kind of competing ground state like Kondo-behaviour[1,2], heavy fermion superconductivity[3], fluctuating valance state (Ce, Eu, Yb)[4]. Recently, intermetallic compounds with *RE* elements as one of its constituent elements drawing more focus because of capability of adopting different crystallographic structures, which in turn influence their physical and chemical properties. Solid solution based on *RE* also shows some very interesting physical properties similar to intermetallics[5–7]. It is well known that, in strongly correlated *f*-electron systems, there is a competition between Ruderman-Kittle-Kasuya-Yosida (RKKY) interaction and Kondo effect. The former promotes the long–range magnetic ordering of localized 4*f* electron spins and quenching of magnetic moments of 4*f* electrons is enhanced by Kondo effect. RKKY interaction dominates Kondo effect in magnetically ordered systems whereas in non–magnetic valence fluctuating systems RKKY interaction is dominated by Kondo effect which in turn realizing heavy fermion behaviour. Ytterbium based compound used to behave some very unusual physical properties owing to its energetically close oxidation states Yb^{2+} and Yb^{3+}. Due to this it shows the mixed valance state which in turn increases the completion between RKKY and Kondo effect resulting different interesting physical properties.

In this view, realizing magnetically ordered Kondo lattices is of the fundamental interest in strongly correlated *f*-electron systems. Numerous investigations were done on magnetic and heavy fermion behaviour of cerium and uranium based intermetallic compounds. Because of electron-hole analogy between electronic configuration of Ce^{3+} ($4f^1$) and Yb^{3+} ($4f^{13}$), extensive research was done on ytterbium based intermetallic compounds exhibiting valence fluctuations. These valence fluctuations lead to partly itinerant and localized character of 4*f* electrons present in Yb and provide an extra charge degree of freedom, which in turn exhibit diverse physical properties in these compounds.

3.2 Experimental

3.2.1 Synthesis

All the compounds were prepared by as purchased high pure metals Yb, Co, Ca and In from Alfa Assar.. Stoichiometric amounts of these metals were weighed and transferred into niobium ampules and were sealed under argon atmosphere by arc melting apparatus (Edmund Biuhler Gmbh compact arch melter MAM-1). These sealed tubes were placed in a water cooled sample holder attached to an induction melting unit (EasyHeat Induction heating system, model 7590). In the typical synthesis, initially we rapidly increased the temperature to 1273 K within 2 min and samples were kept at that temperature for a period of 20 min, then cooled to 1123 K within 2 min. Samples were maintained at that temperature for 30 min and finally cool down to room temperature suddenly by switching off the power button. We could not observe any reaction between niobium tube and the samples. All the samples separated from niobium tube were ground into fine powder and was used to perform all the characterization techniques.

3.2.2 Powder X-ray diffraction

Phase purity of all the synthesized compounds were confirmed by collecting powder X-ray diffractograms using Bruker D8 Discover diffractometer. Cu K_α radiation (λ = 1.5406 Å) was used to perform all these experiments. All the samples were scanned for 1 hr in the 2θ range of 10–90^o with a step size of 0.02^o.

3.2.3 Resistivity

Temperature dependence of DC resistance (2-300 K) measurement was carried out on all the compounds using a standard linear four probe method through an embedded ARS cryostat, which has been controlled by a LabView program, Keithley 2400 C source meter and Lakeshore 336 temperature controller. Resistance data was collected during the cooling cycle. Current of 1 mA was applied through two 0.5 μ copper wires. All these measurements were performed on sintered pellets of dimensions (8.3 mm × 1.6 mm). The observed resistance data was converted into resistivity by using the standard relation between resistance and resistivity.

3.2.4 Magnetic measurements

Magnetic measurements were done on all the samples using Quantum Design Superconducting Quantum Interference Device (QD–SQUID) magnetic property measurement system (MPMS). Temperature dependent magnetic susceptibility was collected both in Zero Field Cooled (ZFC) and Field Cooled (FC) modes at an applied field

of 1000 Oe. Field dependent magnetization measurements were also done at room temperature.

3.3 Results and Discussion

3.3.1 Power X-ray Diffraction (PXRD)

PXRD patterns of $Yb_2Co_{1-x}In_{3+x}$ (x = 0.0, 0.1, 0.2, 0.4, 0.5 and 0.6) and Ca_2CoIn_3 are shown in **Figure 3.1**.

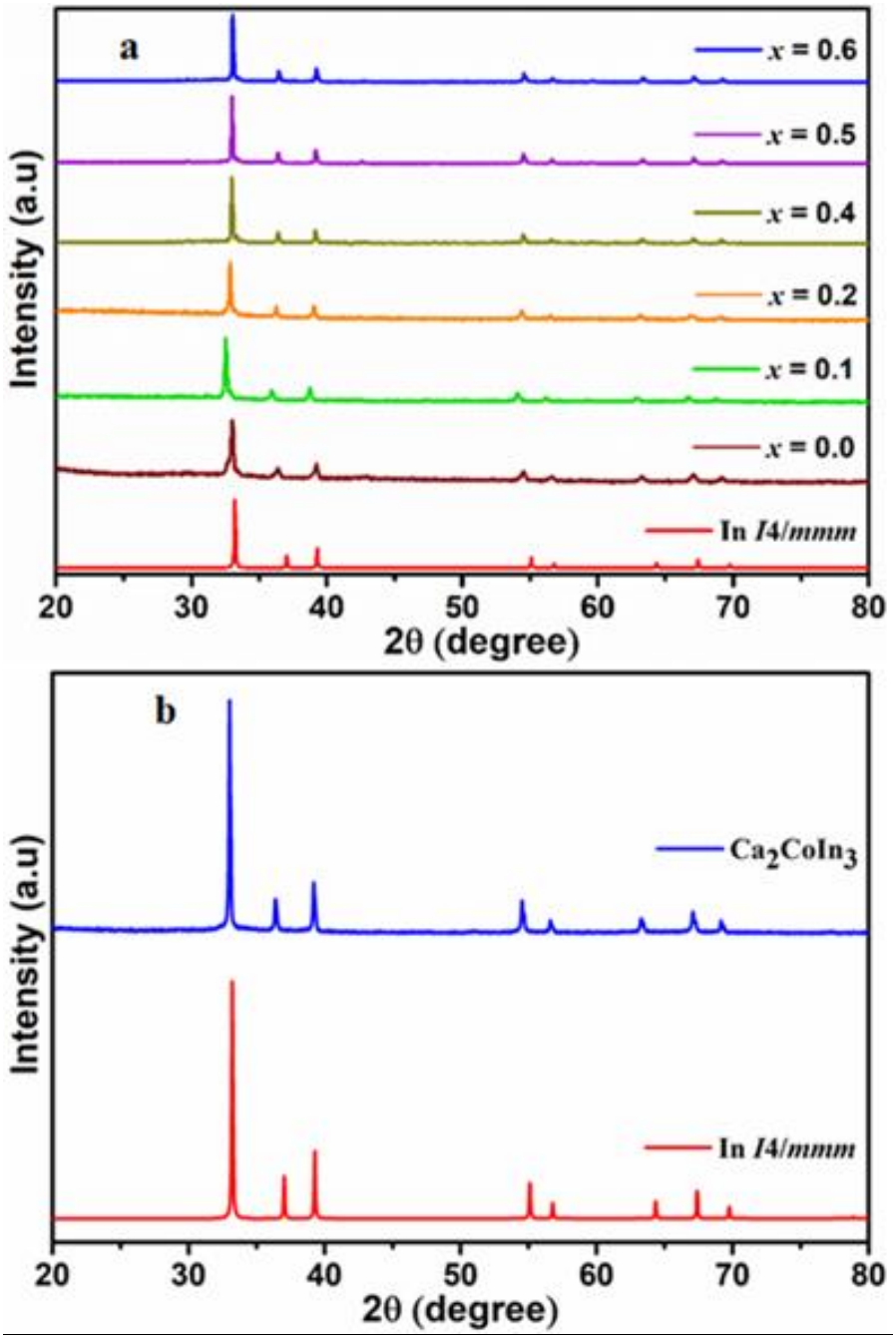

Figure 3.1. Powder XRD of (**a)** $Yb_2Co_{1-x}In_{3+x}$ (x = 0-0.6) and (**b)** Ca_2CoIn_3 compounds

Interestingly, all these compounds observed to crystallize in metallic indium type structure. All the reflections were well indexed with In metal tetragonal structure with *I*4/*mmm* space group. According to Hume-Rothery rule, solid solution can form when the difference between solvent and solute atoms radius is less than 15%, both components exist in same structure type, lesser the electronegativity difference, solubility of metal with higher valance should be more than metal of low valency the vice-versa. In $Yb_2Co_{1-x}In_{3+x}$, size difference of atoms is less than 15% (Yb- 228 pm, Co- 200 pm, In- 220 pm), electronegativity difference of these elements is also small but In metal crystallizes in space group *I*4/*mmm* while Yb and Co metal crystallises in $P6_3/mmc$ space group. So, $Yb_2Co_{1-x}In_{3+x}$ is forming a solid solution, however it is not following one of the criteria above mentioned criteria to be classified as Hume-Rothery phase. They are further classified as interstitial and substitutional solid solution. In powder XRD of $Yb_2Co_{1-x}In_{3+x}$ all the peaks position and intensity ratio are matching with In metal powder XRD. This indicates that all the Yb and Co atoms are uniformly occupying the In metal lattice position and makes this ordered substitutional solid solution. If there is any interstitial occupation by Yb or Co metal, there should be elemental peaks of corresponding metal in powder XRD which we didn't observe in powder XRD data and that is different form In metal. To get insight of magnetic contribution of Yb metal in Yb_2CoIn_3 we also synthesized isostructural Ca_2CoIn_3 (Ca atomic size 231 pm) with the same synthetic condition as evident form **Figure 3.1b**. On increasing the In content in all the powder XRD peaks shifts to higher 2θ value.

3.3.2 Electrical Resistivity

Temperature dependent resistivity of compounds was measured in the range 2 – 300 K using standard linear four probe technique and is shown in **Figure 3.2**. Resistivity is decreasing monotonically in the temperature range of 300 K to ~4 K confirms the metallic behaviour of all the samples. At room temperature (300 K), the compounds $Yb_2Co_{1-x}In_{3+x}$ (x = 0, 0.2 and 0.4) possess 2.045×10^{-4} Ω cm, 1.961×10^{-4} Ω cm and 1.914×10^{-4} Ω cm resistivity values respectively. Resistivity is decreasing with decreasing the Co concentration. There is a non-monotonic variation below 5 K (see inset of **Figure 3.2**) where the resistivity reaches a minimum value 1.9×10^{-7} Ω. cm at 4.27 K and a slight increase in resistivity was observed below 4.27 K. This might be attributed to the formation of coherent Kondo state due to which resistivity will be increased by scattering of conduction electrons which is also observed for other Yb based compound[5,8,9]. Thus, our resistivity measurements indicate the Kondo kind behaviour.

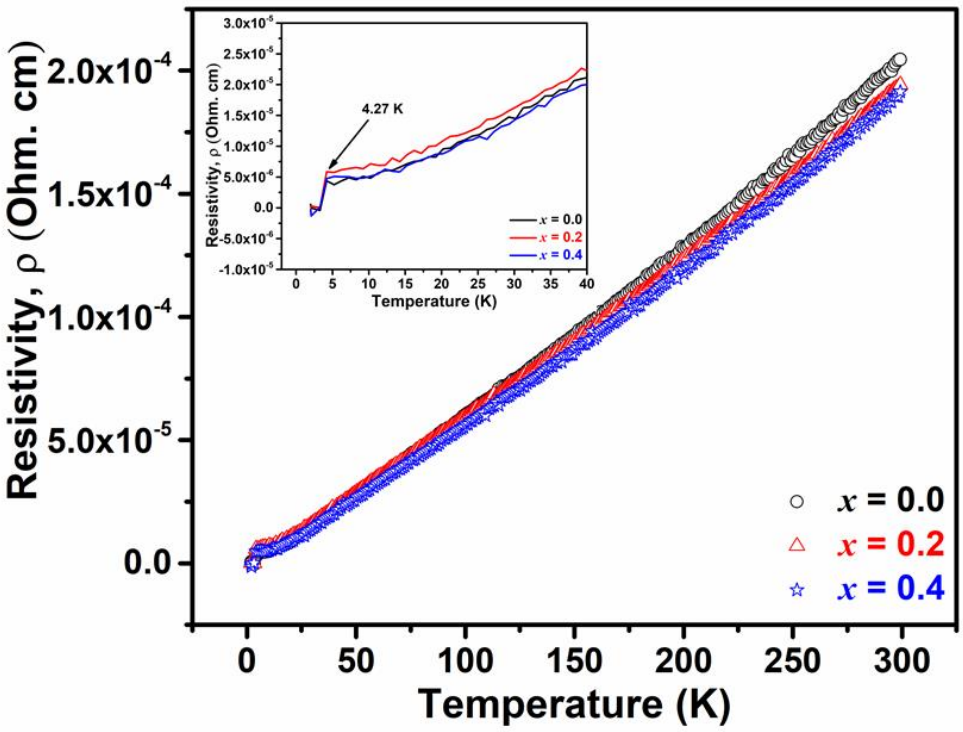

Figure 3.2. Electric resistivity in the temperature range 2-300 K showing metallic behaviour above ~ 4 K.

3.3.3. Magnetic properties

Figure 3.3a shows the temperature dependent susceptibility of $Yb_2Co_{1-x}In_{3+x}$ (x = 0, 0.1, 0.2, 0.4, 0.5 and 0.6) compounds at an applied field of 1000 Oe. In temperature range of 150 to 300 K susceptibility first increase slightly and slowly decreases till 20 K and then sudden jump in susceptibility at low temperature. These type of non-linearity in susceptibility curve associated with mixed valance of constituent elements. Ytterbium can exists in Yb^{2+} and Yb^{3+} oxidation states in $4f^{13}$ and $4f^{14}$ electronic configuration, respectively[5,10]. Weak temperature dependence of susceptibility in the temperature range of 20-300 K for Yb_2CoIn_3 indicates predominantly Yb is in non-magnetic +2 oxidation state while in the range lower temperature range Yb is in +3 oxidation state. All other compounds exhibit the same phenomenon as the pristine one. But on decreasing the Co concentration non-linearity is getting reduces showing that in higher temperature range there are some fraction of Yb^{3+} ions also exist in higher temperature region. Variation in susceptibility with varying the Co concentration implies that Co magnetic moment playing crucial role.

The sudden upturn in susceptibility in the low temperature range is also observed in some Kondo lattice with ferromagnetic ordering show[11–14]. Susceptibility also varies with Co concentration and can be inferred from **Figure 3.3b**. On decreasing the Co

concentration upturn in susceptibility is moves to higher temperature. This observation indicating, magnetic moment direction of Yb and Co atoms are opposite direction in all $Yb_2Co_{1-x}In_{3+x}$ (x = 0, 0.1, 0.2, 0.4, 0.5 and 0.6) which was also confirmed from the magnetization data are discussed below.

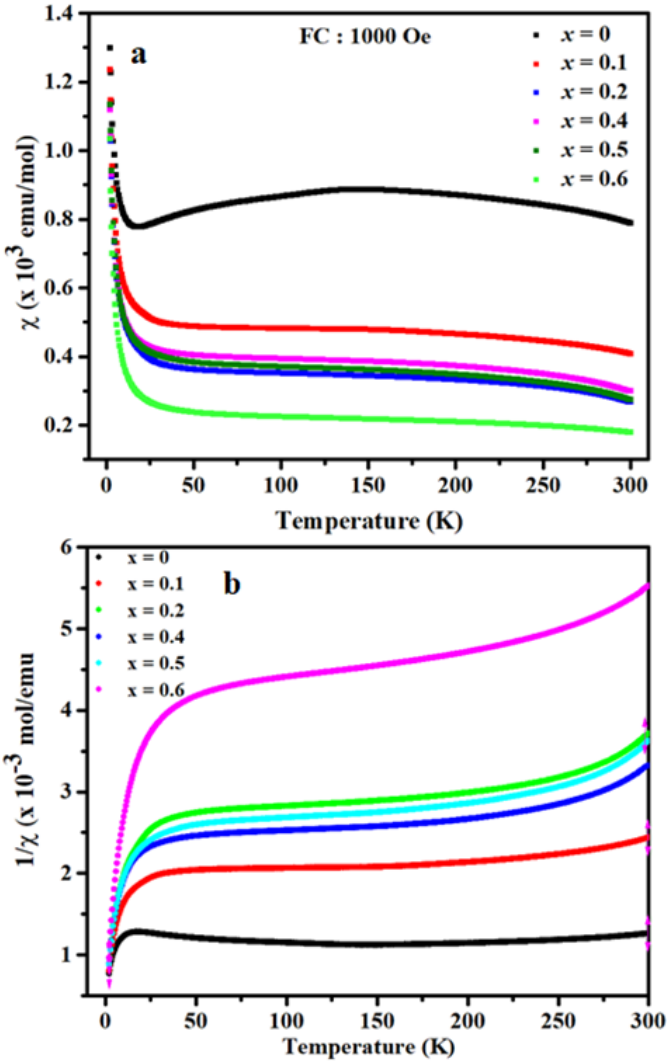

Figure 3.3. Temperature dependant susceptibility **(a)** and temperature dependent susceptibility (b) data for $Yb_2Co_{1-x}In_{3+x}$ (x = 0, 0.1, 0.2, 0.4, 0.5 and 0.6) showing non-linear behaviour in entire temperature range.

Field dependent room temperature magnetization of $Yb_2Co_{1-x}In_{3+x}$ (x = 0, 0.1, 0.2, 0.4, 0.5 and 0.6) compounds is shown in **Figure 3.4a.** Hysteresis behaviour in all these compounds confirms ferromagnetism at room temperature. Origin of ferromagnetism in all these solid solutions can be attributed to presence of unpaired 4*f* -electron in Yb^{3+} along with presence cobalt atom. However, there is no saturation in magnetization ever after applying 6 T and might be due to the crystalline electric field. Highest magnetization of 0.55 μ_B/*f*.u was observed at 6 T for pristine compound. Decrease in magnetization was

observed with increasing the values of '*x*' and can be attributed to decrease in the concentration of cobalt in these compounds. On the hand, the observed coercive field in all these compounds is much higher than metallic cobalt and are given in **Table 3.1**. Pristine compound shows highest coercive field (except for x = 0.6 case) of 751.8 Oe which is around 4 times higher than metallic cobalt, which confirms that the origin of ferromagnetism in these compounds is inherent.

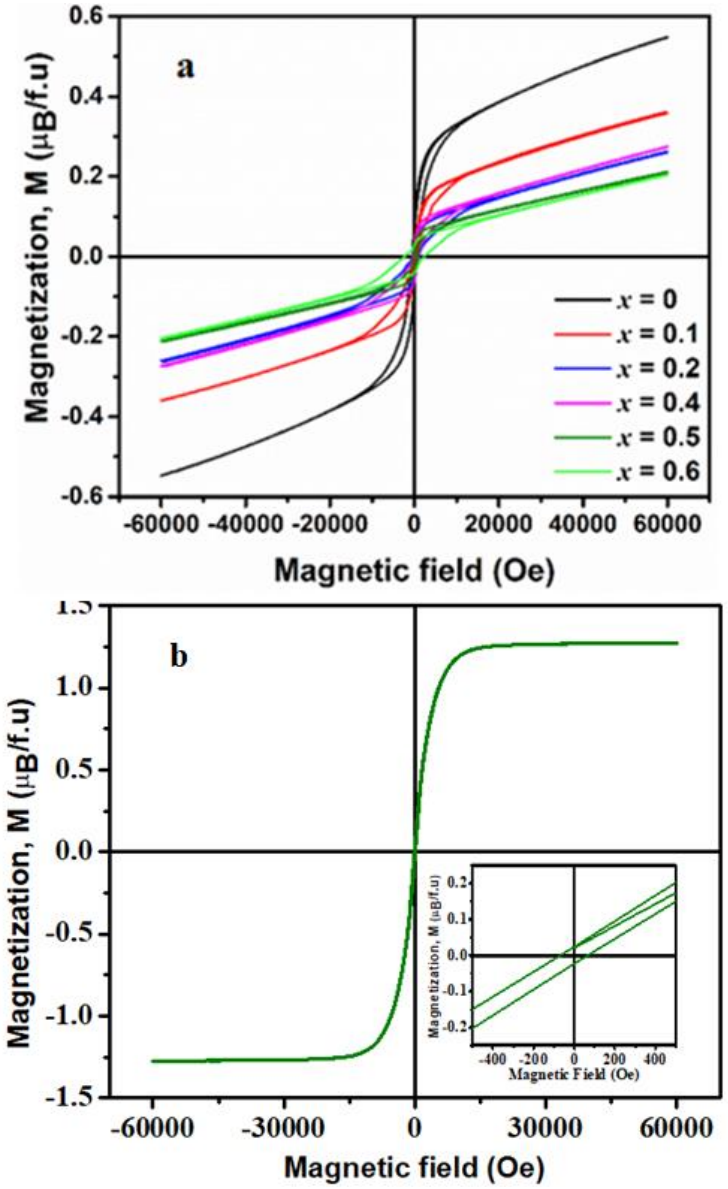

Figure 3.4. Magnetization curve at 300 K for **(a)** $Yb_2Co_{1-x}In_{3+x}$ (x = 0, 0.1, 0.2, 0.4, 0.5 and 0.6) and **(b)** Ca_2CoIn_3.

In order to understand the contribution of Yb to the magnetic properties of these compounds, we have prepared another compound by replacing Yb with non-magnetic Ca. Surprisingly, Ca_2CoIn_3 also exhibited ferromagnetic behaviour at room temperature (See

Figure 3.4b). More interestingly, saturation in magnetization was observed at lower applied magnetic fields. A saturation magnetization (M_s) of 1.28 μ_B/*f*.u was observed in Ca_2CoIn_3 which is very close to the saturation magnetization of metallic cobalt. This suggesting that the magnetization observed in Ca_2CoIn_3 compound is solely coming from cobalt as other elements are non-magnetic in nature. Magnetization, which we observed in $Yb_2Co_{1-x}In_{3+x}$ (x = 0, 0.1, 0.2, 0.4, 0.5 and 0.6) compounds is much smaller than Ca_2CoIn_3. This might be due to presence additional magnetic moment coming from the unpaired 4*f* electron of Yb^{3+}. Logically, the magnetization should increase if the magnetic moment of unpaired 4*f* electrons aligns in the direction of cobalt magnetic moment within the unit cell.

Table 4.1. Compassion of Coercive field H_c (Oe) and saturation magnetization M (μ_B/ f.u.) for $Yb_2Co_{1-x}In_{3+x}$ (x = 0, 0.1, 0.2, 0.4, 0.5 and 0.6) and Ca_2CoIn_3

Solid Solution	H_c (Oe)	M (μ_B/ f.u)
Yb_2CoIn_3	749.19	0.55
$Yb_2Co_{0.9}In_{3.1}$	531.71	0.36
$Yb_2Co_{0.8}In_{3.2}$	458.69	0.23
$Yb_2Co_{0.7}In_{3.3}$	372.93	0.27
$Yb_2Co_{0.6}In_{3.4}$	163.70	0.211
$Yb_2Co_{0.5}In_{3.5}$	2305	0.03
Ca_2CoIn_3	194.53	1.30

However, the magnetization of Yb_2CoIn_3 (0.55 μ_B/*f*.u) is much lower than metallic cobalt (1.30 μ_B/*f*.u). This suggest that, the magnetic moments arising from unpaired 4*f* electrons and cobalt are aligning in opposite direction, resulting decrease in magnetic moment which in turn lowers the magnetization of $Yb_2Co_{1-x}In_{3+x}$ (x = 0, 0.1, 0.2, 0.4, 0.5 and 0.6) compounds. Low temperature magnetization is also measured and it all of them showing ferromagnetic behaviour but there is some anomaly which still has not been understood completely.

3.4. Conclusion

We are rare reporting a solid solution composed of Yb, Co as solute and In metal as solvent in 213 ratio which crystallises in the *I*4/*mmm* space group. We studied the system by means of temperature dependant resistivity and susceptibility in the temperature range of 2-300 K which indicates sample is metallic in behaviour till 4 K and below that it may form the Kondo lattice and supported from susceptibility in low temperature range. Susceptibility measurement indicates there is mixed valance of Yb atoms in the form of

Yb^{2+} and Yb^{3+}. To confirm the oxidation state, we need to XPS or XANES measurement. It is a rare example of room temperature ferromagnet and remains in the low temperature range also but there is anomaly which has to understood completely (not shown here).

References

(1) Krellner, C.; Kini, N. S.; Brüning, E. M.; Koch, K.; Rosner, H.; Nicklas, M.; Baenitz, M.; Geibel, C. CeRuPO : A Rare Example of a Ferromagnetic Kondo Lattice. *Phys. Rev. B* **2007**, *76*, 104418–10.

(2) Kaczorowski, D. Kondo Lattice Behavior and Magnetic Ordering in $CeRh_2Si_2$. *Phys. Rev. B* **2010**, *81*, 214411–214417.

(3) Mathur, N. D.; Grosche, F. M.; Julian, S. R.; Walker, I. R.; Freye, D. M.; Haselwimmer, R. K. W.; Lonzarich, G. G. Magnetically Mediated Superconductivity in Heavy Fermion Compounds. *Nature* **1998**, *394*, 39–43.

(4) Pandey, S.; Siruguri, V.; Rawat, R. Quantum Critical Point and Intermediate Valence Fluctuations in $CeRu_{2-X}Co_xGe_2$. *Phys. Rev. B*. 2018, 155129–11.

(5) Udumula Subbarao and Sebastian C. Peter. Crystal Structure of YbCu6In6and Mixed Valence Behavior of Yb $InYbCu_{6-x}In_{6+x}$ (X = 0, 1, and 2) Solid Solution. *Inorg. Chem.* **2012**, *51*, 6326–6332.

(6) Sales, B. C.; Jin, K.; Bei, H.; Stocks, G. M.; Samolyuk, G. D.; May, A. F.; Mcguire, M. A. Quantum Critical Behavior in a Concentrated Ternary Solid Solution. *Nat. Publ. Gr.* **2016**, *6*, 1–8.

(7) Search, H.; Journals, C.; Contact, A.; Iopscience, M.; Address, I. P. Yb–Yb Correlations and Crystal-Field Effects in the Kondo Insulator YbB_{12} and Its Solid Solutions. *J. Phys. Condens. Matter* **2004**, *16*, 2631–2646.

(8) Fisher, I. R.; Wiener, T. A.; Bud, S. L.; Canfield, P. C. Thermodynamic and Transport Properties of Single-Crystal $Yb_{14}MnSb_{11}$. *Phys. Rev.* **1999**, *59*, 13829–13834.

(9) Avila, M. A.; Sera, M.; Takabatake, T. $YbNiSi_3$: An Antiferromagnetic Kondo Lattice with Strong Exchange Interaction. *Phys. Rev. B - Condens. Matter Mater.*

Phys. **2004**, *70*, 100409–4.

(10) Search, H.; Journals, C.; Contact, A.; Iopscience, M.; Phys, S. S.; Address, I. P. The Valence State of Yb in $YbXCu_4$, (X = Al, Ag and Ga) Compounds. *J. Phys. C Solid State Phys.* **1987**, *20*, 307–310.

(11) Malik, L. M. and S. K. Ferromagnetic Kondo Lattice Behavior in CeNiSb. *Phys. Rev. B* **1995**, *52*, 35–38.

(12) Zhang, G.-B. L. G.-M. and L. Y. Kondo Screening Coexisting with Ferromagnetic Order as a Possible Ground State for Kondo Lattice Systems. *Phys. Rev. B* **2010**, *81*, 094420-6.

(13) Henning, S.; Nolting, W. Ground-State Magnetic Phase Diagram of the Ferromagnetic Kondo-Lattice Model. *Phys. Rev. B* **2009**, *79*, 064411-7.

(14) Drescher, K.; Abd-Elmeguid, M.M. Micklitz, H.; Sanchez, J. P. Competing Anisotropies in the Ferromagnetic Kondo-Lattice Compound YbNiSn : Observation of a Complex Magnetic Ground State under High Pressure. *Phys. Rev. Lett.* **1996**, *77*, 3228–3231.

Chapter 4

Spin Glass Behavior in Ordered Eu_2AgGe_3

Chapter 4

Spin Glass Behavior in Ordered Eu_2AgGe_3

4.1. Introduction

Magnetic properties have always been critical in case of rare earth (*RE*) based intermetallics. It is the presence of localized f-electron that induces the strong magnetic properties. Interaction between this localized f-electrons through conducting s-electron via Ruderman-Kittel-Kasuya-Yosida (RKKY) oscillatory exchange interaction resulting ferromagnetic (FM) or antiferromagnetic (AFM) ordering in well-ordered crystal structure. Competition between these interaction leads to various kind of phenomenon like superconductivity[1–3], heavy fermions[4,5], Kondo-behaviour[6,7] and spin glass[8–10]. Spin glass behaviour in a material is an example of competing spin interaction that is result of frustration and disorder in the system. Frustration in a system leads to the generation of multiple degenerates or nearly degenerate ground state in the system[11]. Frustration alone cannot lead to the spin glass (e.g. $NiGa_2S_4$ is two-dimensional antiferromagnetic interaction with triangular lattice system)[12]. A triangular lattice cannot show the co-operative frizzing transition on its own[13]. So, it is always desirable to have the disorder as well as frustration in the system to behave as spin glass. Disorder can be of any type like magnetic impurity, random site occupancy or random bond order i.e. changing the interaction in the lattice at nearest neighbour site from ferromagnetic to antiferromagnetic alternatively. However, there are a few exceptions. Ordered stoichiometric compounds like $PrAu_2Si_2$[14] and $PrRuSi_3$[15] show spin glass behaviour even in the absence of lattice frustration or disorder. A prolonged annealing unable to remove spin glass nature of $PrAu_2Si_2$ and $PrRuSi_3$ (spin glass behaviour due to dynamic fluctuations of crystal field levels). URh_2Ge_2[16] is a spin glass material whose glassy behaviour originates from the site disorder of Rh and Ge atoms in lattice can be removed by prolong annealing.

Eu_2AgGe_3 is a member of well-studied RE_2TX_3 (*T*- Transition metal, *X*- Main group element) family[17,18]. There are plenty of compounds reported as spin glass material in this family[17,19–24]. However, interestingly, not a single compound reported for the spin glass behavior. Eu_2AgGe_3 crystallize in the Ba_2LiSi_3 structure type, which is an ordered superstructure of the AlB_2 structure type[25]. Inspired by the above work we investigate the

physical properties of Eu_2AgGe_3. Earlier, Eu_2AgGe_3 was reported for unusual high temperature reversible phase transition[25]. In this study, we report the magnetic susceptibility measurement under various field on polycrystalline Eu_2AgGe_3, which exhibit spin glass transition temperature at 11 K and ferromagnetic ordering at 36 K. This is a rare example of re-entrant spin glass behaviour. Susceptibility measurement coupled with specific heat under no magnetic field confirms ferromagnetic transition at 36 K and spin glass behaviour at 11 K.

4.2. Experimental details

To synthesize Eu_2AgGe_3, Eu (ingots 99.99%, ESPI metals), Ag (ingots, 99.99%, Alfa-Aesar), and Ge (metal pieces 99.999%, Alfa Aesar) were taken in ideal 2:1:3 ratio and weighed in argon gas filled glove box. Stoichiometric amount of the sample was transferred into the tantalum tube and subsequently sealed under argon atmosphere by arc-melting apparatus. Sealed tantalum tube was placed in water cooled high frequency induction furnace instrument followed by heating of the sample with an application current 2.1 Amp/s until186.7 Amp current and kept for 30 minutes followed by annealing of the sample at 155.4 A for 10 minutes with cooling rate 2.1 Amp/s and subsequently quenched by switching off the instrument. A brittle product was found with metallic lustre.

4.2.2 Powder X-Ray Diffraction Powder XRD of sample were taken at using Rigaku D8 venture with Cu Kα wavelength (λ = 1.54187 Å) which confirms the phase purity of the sample and no sign of tantalum tube were reacted with sample within the XRD detection limit.

4.2.3. Magnetic measurements and Specific Heat- Magnetic measurements were carried out in the temperature range 1.72–300 K using a Quantum Design SQUID magnetometer. Specific heat measurements were carried out from 1.8 K to 300 K using relaxation method available in the same PPMS system.

4.3. Results & Discussions

Powder XRD profile fitting (**Figure 4.1)** was done with room temperature phase of Eu_2AgGe_3 having space group *Fddd*. All the reflection was fitted except twin peaks around 2θ value 30° with a = 8.7635 Å , b = 15.0126 Å, c = 17.8241 Å. These twin peaks originated from the small impurity of Eu_3Ag_2 phase[26]. However, Eu_3Ag_2 shows

antiferromagnetic ordering at 61 K, but we didn't observe any anomaly in magnetic susceptibility and specific heat measurements, so we assume that little impurity in powder XRD i.e. Eu_3Ag_2, is very small and not interfering with any other physical properties of Eu_2AgGe_3.

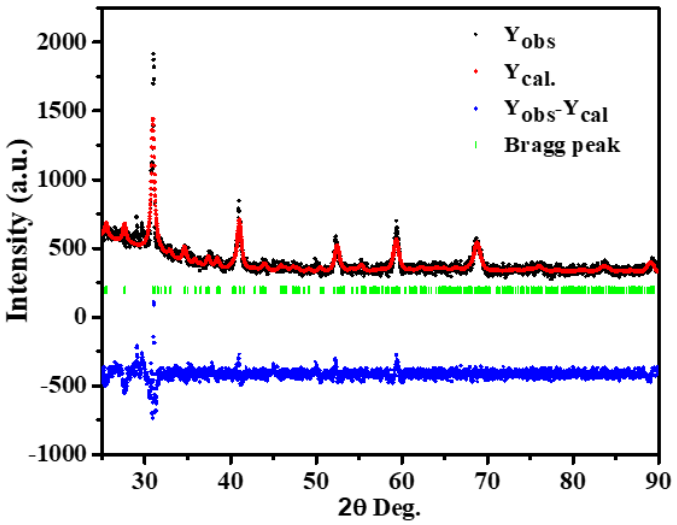

Figure 4.1. Profile fitting of Eu_2AgGe_3 with space group *Fddd.*

There are five non-equivalent crystallographic sites present in the crystal structure of Eu_2AgGe_3 consisting of two Eu sites and three mixed sites with the combination of both Ag and Ge atoms **(Figure 4.2)**.

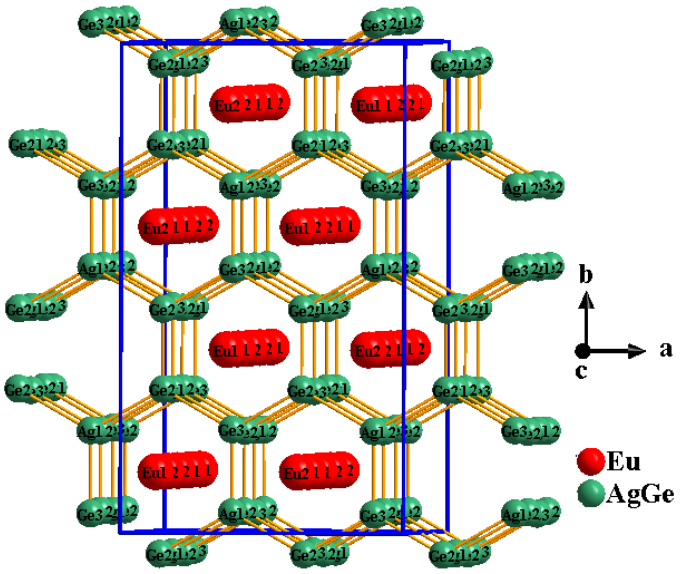

Figure 4.2 Crystal structure of Eu_2AgGe_3, crystallise in orthorhombic crystal system with *Fddd* space group. Cell axis is shown in blue colour

Ag and Ge atoms form indefinite hexagonal layer in *ab* plane with no preferential site occupation. These hexagonal layers are stacked and arranged in ABCD order along the [001] axis. These hexagons are slightly puckered due to the random occupation of Ag and Ge atoms with two crystallographically non-equivalent Eu atoms are sandwiched between them[25]. Due to the puckering of Ag and Ge atoms, hexagonal layers formed by Eu atoms are distorted from their plane. Earlier our group studies Eu Mössbauer and X-ray absorption near-edge spectroscopic (XANES), which confirm the divalent oxidation state of the Eu atoms.

4.3.2 Magentic Measurement- Magnetic susceptibility measurement performed by Sarkar et al. at an applied field of 0.01 Tesla (T) reveals paramagnetic nature of sample above 100 K. Modified Curie-Weiss law ($\chi = C/(T - \theta_P)$) was used to fit the data within the temperature range of 80-325 K gives the paramagnetic Curie temperature, θ_p of 1.8 K[25].

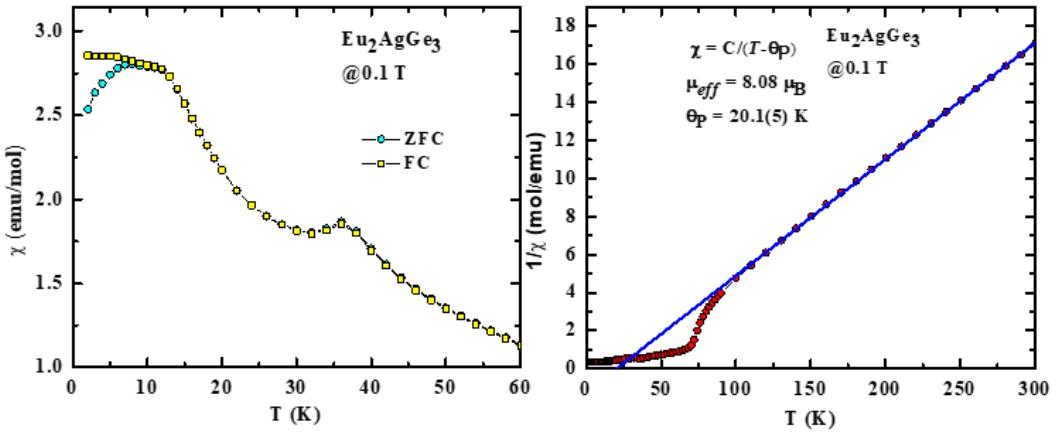

Figure 4.2. (a) The temperature dependence of molar magnetic susceptibility of Eu_2AgGe_3 at 0.1 T applied magnetic field with zero field cooled (ZFC) and field cooled (FC) method. (b) Temperature dependent inverse susceptibility measurement on Eu_2AgGe_3 at applied field of 0.01 T. Blue line indicates the Curie-Weiss fitting in the temperature range 120-300 K.

However, magnetic susceptibility measurement in this work at an applied field of 0.1 T resulted θ_p of 20.1 K **(Figure 4.2b)** and effective magnetic moment of 8.08 μ_B/Eu ion. It is slightly higher than the Eu^{2+} oxidation state magnetic moment value of 7.94 μ_B/Eu free ion, which is due to conduction electron polarization[27]. Difference between θ_p value is due to the difference in data fitting. Positive value of θ_p indicates there is ferromagnetic interactions in the Eu_2AgGe_3, which is expected for any spin-glass

materials[10,17]. Deviation from Curie-Wiess law below 120 K probably due to crystalline electric field effect[19].

ZFC and FC magnetic susceptibility measurement at 0.01 T and ZFC under different applied magnetic field are plotted in **Figures 4.3a** and 4.**3b**, respectively. In **Figure 4.3a,** one can observe the bifurcation in ZFC and FC curve below 70 K. In ZFC the magnetic ion (Eu^{2+}) starts to freeze randomly with no directionality while in case of FC the magnetic ions try to align in the easy direction owing to lower energy in the system, on decreasing the temperature. This type of bifurcation indicates that system might be a probable candidate of spin-glass behavior[10,23,28]. There is sudden upturn in susceptibility data around 70 K and after a sudden dip around 36 K.

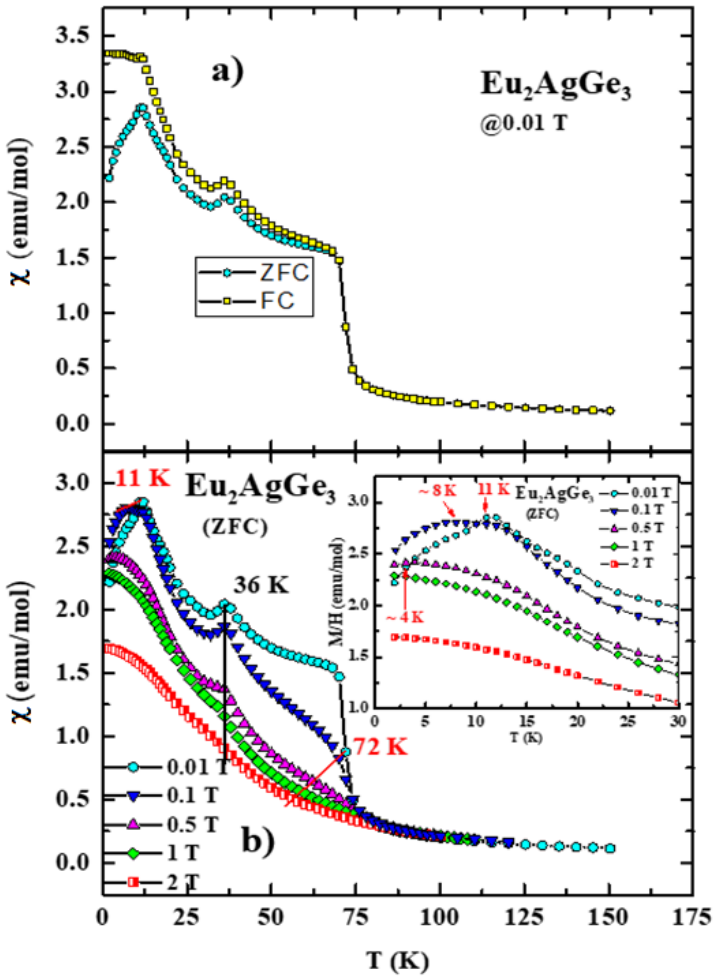

Figure 4.3. (a) DC magnetic susceptibility measurement under applied field of 0.01 T, (**b)** ZFC measurement under different applied filed. Inset showing lowering of spin glass transition on increasing magnetic field.

There is irreversibility in ZFC and FC curve below 70 K which will name as T_{Irr}, while nature of peak around 36 K is characteristic of ferromagnetic ordering will name as,

T_F. Saturation of FC curve, which is almost independent of temperature and decrease in susceptibility in ZFC curve below 11 K, is unique feature of any spin glass system and will name this as T_{S-G}.

Peaks at 11 K and 70 K under different applied magnetic field moves towards the lower temperature upon increasing the field and is given in **Table 4.1.** According to mean field theory in typical Heisenberg spin glass system, there are two different type of weak and strong irreversibility lines occur in H-T diagram namely de Almeida-Thouless (AT) line and Gabay-Thouless (GT) line, respectively[29,30]. According to mean field theory AT line separates the spin glass to paramagnetic phase. However, here we don't have enough data point to plot AT and GT curve. To get the enough data point the additional experiments are under progress.

Peak around 11 K is going down to lower temperature and can be seen up to 0.5 T field but not below that, as data point are not sufficient to claim. To confirm this hypothesis, we need to measure the dc susceptibility down to milli kelvin range. Lowering of peak position in dc susceptibility upon decreasing the temperature is clear indication of spin-glass behaviour in Eu_2AgGe_3. These type of behaviour is generally associated with canonical spin glass system[31]. However, disparity in ZFC and FC dc susceptibility curve is not enough condition to claim to a system as spin glass. U_2RhSi_3 reported for bifurcation in ZFC and FC curve but there was no sign of spin glass behaviour in ac susceptibility measurement and bifurcation was attributed to ferromagnetic domain wall pinning effect[32]. So, ac susceptibility with varying frequency is needed to confirm the spin glass behaviour.

Table 4.1. Shift in peak position in ZFC and FC measurement under applied magnetic field of 0.01T

Applied Magnetic Field Tesla (T)	**T_{Irr}**	**T_{S-G} Kelvin (K)**
0.01	70	11
0.1	11	~ 8
0.5	------	~ 4
1.0	------	------
2.0	------	------

Surprisingly, there is no field dependence of peak around 36 K in the susceptibility measurement. Just the peak is broadened but not shifting with increasing magnetic field, which is complete proof that there is magnetic ordering and nature of peaks confirm the ferromagnetic interaction. This is confirmed by specific heat

measurements as well, which will be discussed later. It is very unusual example of re-entrant spin glass in Eu based intermetallics where first observing ferromagnetic ordering and on further cooling to spin-glass

This reentrant behaviour can be understood by frustration and disorder in the system. The Eu-Eu inter-layer and intra-layer distance are ranges in 4.41-4.45 Å and 4.33-4.35 Å, respectively. So nearest neighbour interaction (NNI) will be the intra-layer Eu^{2+} ions and next nearest neighbour interaction (NNNI) will comes from inter-layer Eu^{2+} ions. Let's name NNI and NNNI coupling constant as J_1 and J_2, respectively. To satisfy the spin glass behaviour J_1 and J_2 should have different sign. If $J_1 > 0$ and $J_2 < 0$, ferromagnetic ordering of Eu^{2+} ion expected in *ab*-plane and antiferromagnetic ordering in [001] axis. This type of mechanism also provided for structurally similar intermetallic Ce_2CuGe_3[32]. Since there is ferromagnetic ordering around 36 K that indicates $|J_1| > |J_2|$ around that temperature. In lower temperature range there is spin glass transition that indicate the average value of exchange coupling constant is zero. This can be due to shortening of inter-layer distance and leads to $|J_1| = |J_2|$. In a periodic lattice, disorder is induced by mixed occupation site in the lattice. Random site occupation of Ag/Ge atoms in Eu_2AgGe_3 at three Wyckoff position 16*f*, 16*f* and 32*h* give rise to RKKY exchange coupling[19]. Magnetization measurement were done at 1.8 K in varying magnetic field **Figure 4.4**.

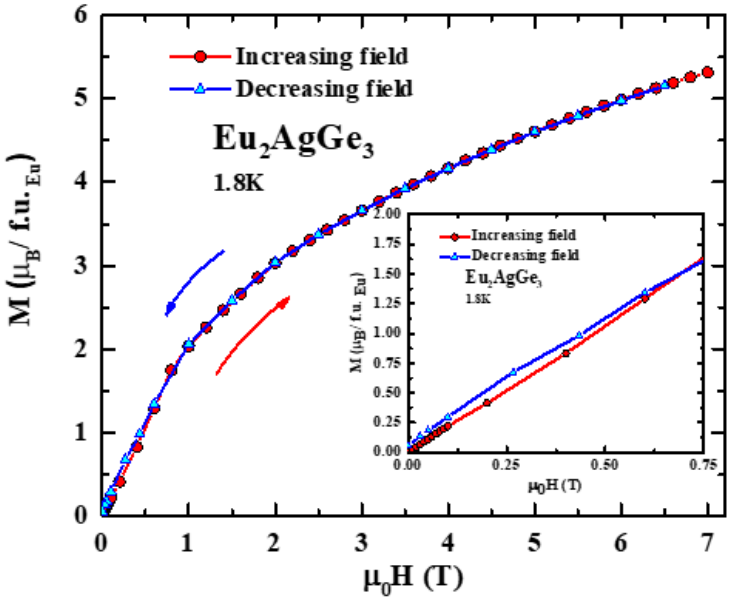

Figure 4.4. Magnetization curve of Eu_2AgGe_3 at 1.8 K. Inset represents enlarged view of the magnetization curve in the magnetic field range of 0 to 0.75 T.

In low magnetic field region slope were high while in higher magnetic field region there is decrease in slope and it is looks like magnetization is not going to saturate in even higher magnetic field. It shows very small hysteresis in low magnetic field i.e. less than 0.75 T. This hysteresis may come from the ferromagnetic domain wall frizzing in low temperature.

4.3.3. Specific Heat -Specific heat of a materials can be expressed as $\mathbf{C = C_e + C_{la} + C_m}$, where C is total specific heat, C_e, C_{ph} and C_m are the electronic (linear in T), lattice vibration (proportional to T^3) and magnetic specific heat (In case of spin glass, $T < T_f$ is linear in T), respectively. To calculate magnetic contribution of specific heat one need to subtract the electronic and lattice vibration part from total specific heat, and it can be achieved by replacing the magnetic ion by any non-magnetic ion with same structure. Specific heat measurement of isostructural non-magnetic contuerpart Ba_2AgGe_3 is under progress.

The result of specific heat under no magnetic field is plotted in **Figure** 4.**5a** and 4.**5b** as C vs T and C/T vs T, respectively. Magnetic ordering around 36 K evident from λ-like anomaly. Specific heat coupled with magnetic field dependant ZFC dc susceptibility measurement confirm ferromagnetic ordering around 36 K. In **Figure 4.5a**, inset there is broad peak centre around 11 K is observed which also indicates that there is no long-range magnetic ordering.

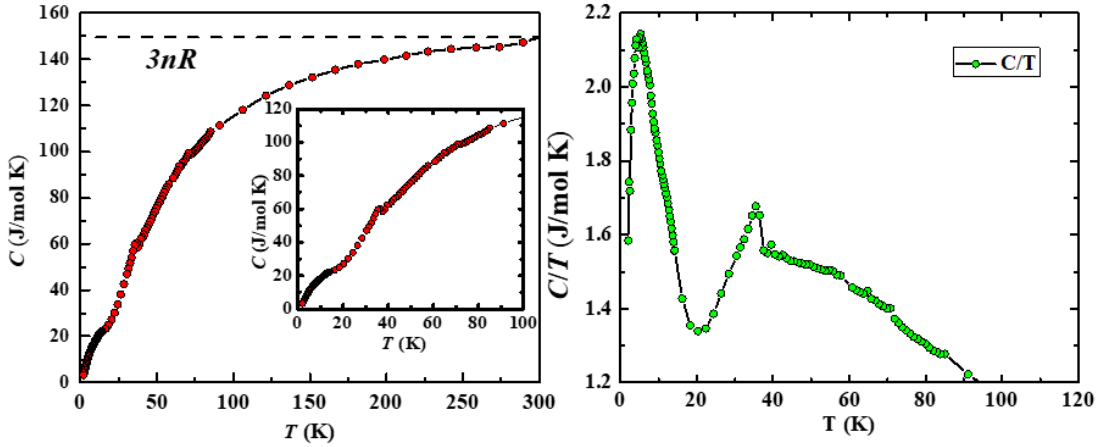

Figure 4.5 a) Temperature dependant specific heat measurement from 2 K to 300 K. Inset of figure **a** is low temperature specific heat. **b)** C/T vs T in low temperature range.

The Eu-Eu inter-planner and intra-planner distance are ranges in 4.41-4.45 Å and 4.33-4.35 Å, respectively while in Eu metal is 3.27-3.36 Å. Larger separation between Eu atoms in Eu_2AgGe_3 as compared to its metallic form leads the localization of *f*-electron on Eu atoms, therefore very less *f*-orbital overlap in Eu_2AgGe_3. Localization of *f*-electrons

leads to polarise the conducting electron and hinders the movement and resulting heavy mass of conducting electrons. Due to random occupation of Ag/Ge atoms produces the varying electronic environment around Eu atoms and induces the varying RKKY interaction.

4.4 Conclusion

In conclusion, our study on polycrystalline Eu_2AgGe_3 through varying ZFC and FC susceptibility measurement with different applied magnetic field and specific heat under with zero field give the clear indication of spin glass behaviour around 11 K and ferromagnetic ordering around 36 K. To confirm the spin glass behaviour, ac susceptibility with varying frequency is required. To get the nature of spin glass either it is Ising or Heisenberg system, need to measure ZFC and FC curve with low applied magnetic field with very small step size. Interesting point is that it exhibits reentrant spin glass behaviour.

4.4 References

(1) Tran, V. H.; Kaczorowski, D.; Khan, R. T.; Bauer, E. Superconductivity and Non-Fermi-Liquid Behavior of Ce_2PdIn_8. *Phys. Rev. B* **2011**, *064504*, 1–6.

(2) Sokolov, D. A.; Aronson, M. C.; Henderson, C.; Kampf, J. W. Crystalline Electric Fields and the Ground State of Ce_3RhPb_{13}. *Phys. Rev. B* **2007**, *76*, 3–6.

(3) Steglich, F.; Aarts, J.; Bredl, C. D.; Lieke, W.; Meschede, D.; Franz, W. Superconductivity in the Presence of Strong Pauli Paramagnetism: $CeCu_2Si_2$. *Phys. Rev. Lett.* **1979**, *437*, 1892–1896.

(4) Taylor, P. Heavy-Fermion Intermetallic Compounds. *Contemp. Phys.* **2006**, *28* (1987), 143–157.

(5) Honda, F.; Hirose, Y.; Malik, S. K.; Adroja, D. T. Related Content Magnetic and Transport Properties of Heavy Fermion Compound CePtSi. *Jpn. J. Appl. Phys.* **1987**, *26*, 551–552.

(6) Handbook on the Physics and Chemistry of Rare Earths, Edited by K.A. Gschneidner, Jr. and L. Eyring North-Holland Publishing Company; 1978; pp 798–823.

(7) Hundley, M. F.; Sarrao, J. L.; Thompson, J. D.; Movshovich, R.; Jaime, M.

Unusual Kondo Behavior in the Indium-Rich Heavy-Fermion Antiferromagnet $Ce_3Pt_4In_{13}$. *Phys. Rev. B* **2001**, *65*, 1–7.

(8) Paulose, P. L.; Sampathkumaran, E. V.; Bitterlich, H.; Behr, G.; Löser, W. Anisotropic Spin-Glass-like and Quasi-One-Dimensional Magnetic Behavior in the Intermetallic Compound Tb_2PdSi_3. *Phys. Rev. B - Condens. Matter Mater. Phys.* **2003**, *67*, 1–4.

(9) Pronin, A. V.; Neubauer, D.; Cao, G. H.; Dressel, M.; Baumgartner, A.; Zapf, S.; Jiao, W. H. Reentrant Phases in Electron-Doped $EuFe_2As_2$: Spin Glass and Superconductivity. *Phys. Rev. B* **2017**, *95*, 1–11.

(10) Rayaprol, S.; Pöttgen, R. Gd_2Au_2Cd: A Mo_2FeB_2 -Type Intermetallic with Ferromagnetic Ordering and Spin Glass Anomalies. *Phys. Rev. B - Condens. Matter Mater. Phys.* **2006**, *73*, 214403–214408.

(11) Maletta, H. Handbook on the Physics and Chemistry of Rare Earths, Vol. 12 Edited by K.A. Gschneidner, Jr. and L. Eyring © Elsevier Science Publishers B.V.; 1989; Vol. 12, pp 343–461.

(12) S. Nakatsuji; Y. Nambu; H. Tonomura; O. Sakai; S. Jonas; C. Broholm; H. Tsunetsugu; Y. Qiu; Maeno, Y. Spin Disorder on a Triangular Lattice. *Science* **2005**, *309*, 1697–1700.

(13) Mydosh, J. A. *Spin Glasses : An Experimental Introduction*; 1993.

(14) Macaluso, R. T.; Rainford, B. D.; Adroja, D. T.; Osborn, R.; Goremychkin, E. A.; Koza, M. Spin-Glass Order Induced by Dynamic Frustration. *Nat. Phys.* **2008**, *4*, 766–770.

(15) Anand, V. K.; Adroja, D. T.; Hillier, A. D.; Taylor, J.; André, G. Signatures of Spin-Glass Behavior in the Induced Magnetic Moment System $PrRuSi_3$. *Phys. Rev. B - Condens. Matter Mater. Phys.* **2011**, *84*, 1–10.

(16) Süllow, S.; Mentink, S.; Mason, T. Disorder to Order Transition in the Magnetic and Electronic Properties. *Phys. Rev. B - Condens. Matter Mater. Phys.* **2000**, *61*, 8878–8887.

(17) Pan, Z. Y.; Cao, C. De; Bai, X. J.; Song, R. B.; Zheng, J. B.; Duan, L. B. Structures and Physical Properties of R_2TX_3 Compounds. *Chin. Phys. B* **2013**, *22*, 056102-10.

(18) Hoffmann, R.-D.; Pöttgen, R. AlB_2-Related Intermetallic Compounds-a Comprehensive View Based on Group-Subgroup Relations. **2001**, *216*, 127–145.

(19) Nishioka, T.; Tabata, Y.; Taniguchi, T.; Miyako, Y. Canonical Spin Glass Behavior in Ce_2AgIn_3. *J. Phys. Soc. Japan* **2000**, *69*, 1012–1015.

(20) Homma, Y.; Yamamoto, E.; Onuki, Y.; Honma, T.; Kimura, Y.; Haga, Y.; Shiokawa, Y.; Li, D. X.; Dönni, A. Spin-Glass Behaviour with Extended Short-Range Ferromagnetic Order in U_2RhSi_3. *J. Phys. Condens. Matter* **2002**, *11*, 8263–8274.

(21) Nimori, S.; Shikama, T.; Kimura, A.; Li, D. X.; Haga, Y. Magnetic Anisotropy and Spin-Glass Behavior in Single Crystalline U_2PdSi_3. *J. Phys. Condens. Matter* **2011**, *23*, 076003-7.

(22) Li, D. X.; Yamamura, T.; Yubuta, K.; Nimori, S.; Haga, Y.; Shikama, T. Evidence for Spin-Glass State in Nonmagnetic Atom Disorder Compound Pr_2AgIn_3. *J. Phys. Conf. Ser.* **2011**, *320-329*.

(23) Li, D. X.; Nimori, S.; Ohta, S.; Yamamura, Y.; Shikama, Y. Random Spin Freezing in Single Crystalline Ce_2CuSi_3. *J. Phys. Conf. Ser.* **2012**, *400*, 032044.

(24) Tang, C. C.; Gao, X. Q.; Shen, B. G.; Shen, J.; Liu, Y.; Sun, J. R.; Hu, F. X.; Wu, J. F.; Mo, Z. J. Magnetic Properties and Magnetocaloric Effect in the R_2PdSi_3 (R=Gd, Dy and Er) Compounds. *J. Alloys Compd.* **2014**, *626*, 145–149.

(25) Sarkar, S.; Peter, S. C. Structural Phase Transitions in a New Compound Eu_2AgGe_3. *Inorg. Chem.* **2013**, *52*, 9741–9748.

(26) K.H.J. Buschow, H. W. W. V. D. Note on the Formation and the Magnetic Propeties of Amporphus Eu-Ag Alloys. *J. Magn. Magn. Mater.* **1979**, *12*, 123–126.

(27) Arons, R. R.; Siouris, I. M.; Semitelou, I. P.; Yakinthos, J. K.; Schafer, W. Magnetic Structure of Tb_2CuIn_3. *J. Alloys Compd.* **2001**, *314*, 1–6.

(28) Li, S.; Wang, Z.; Chen, G.; Chen, X. Double-Peak Specific Heat and Spin Freezing in the Spin-2 Triangular Lattice Antiferromagnet $FeAl_2Se_4$. *Phys. Rev. B* **2019**, *054421*, 1–8.

(29) Gabay, M.; Toulouse, G. Coexistence of Spin-Glass and Ferromagnetic Orderings.

Phys. Rev. Lett. **1981**, *47*, 201–204.

(30) Almeida, J. De; Thouless, D. Stability of the Sherrington-Kirkpatrick Solution of a Spin Glass Model. *J. Phys. A Math. Gen.* **1977**, *11*, 983–990.

(31) Haga, Y.; Nimori, S.; Onodera, H.; Ōnuki, Y.; Tobo, A.; Shiokawa, Y.; Yamamoto, E.; Li, D. X. Spin-Glass Behavior with Short-Range Antiferromagnetic Order in Nd_2AgIn_3. *Appl. Phys. Lett.* **2002**, *79*, 4183–4185.

(32) Chevalier, B.; Pöttgen, R.; Darriet, B.; Gravereau, P.; Etourneau, J. Structural Chemistry and Magnetic Behaviour of the Ternary Silicides U_2TSi_3 (T = Mn, Fe, Co, Ni, Ru, Rh, Pd, Os, Ir, Pt, Au). *J. Alloys Compd.* **1996**, *233*, 150–160.

(33) Stewart, G. R. Heavy-Fermion Systems. *Mater. Sci. Technol. Diuision* **1979**, No. 1979.